 CMES, vol.24, no.1, pp.21-50, 2008

A Hybrid Sensitivity Filtering Method for Topology Optimization

S.Y. Wang[1,2] , K.M. Lim[2,3], B.C. Khoo[2,3] and M.Y. Wang[4]

Abstract: In topology optimization, filtering techniques have become quite popular in practice. In this paper, an accurate and efficient hybrid sensitivity filtering approach based on the traditional and bilateral sensitivity filtering approaches is proposed. In the present hybrid approach, the traditional sensitivity filter is applied to a subdomain where numerical instabilities are likely to occur to overcome the numerical instabilites robustly. Filtering on mesh-independent holes identified by an image-processing-based technique is prohibited to reduce the computational cost. The bilateral approach is employed for the corresponding nearest neighboring elements of the mesh-independent holes to drive the 0-1 convergence of their boundaries. As a result, the optimal designs can be checkerboard-free, mesh-independent and mostly black-and-white. The possible side effects of the traditional and bilateral sensitivity filtering approaches can be alleviated. Existence of solutions can be ensured in a more accurate manner. The high accuracy and efficiency of the present approach are illustrated with classical examples in minimum compliance design. It is suggested that the present hybrid approach for topology optimization be highly appealing.

Keyword: Topology optimization, sensitivity filter, bilateral filter, numerical instabilities, existence of solutions, black-and-white designs

[1] Corresponding author, Email: smaws@nus.edu.sg.
[2] Singapore-MIT Alliance, E4-04-10, 4 Engineering Drive 3, Singapore 117576.
[3] Department of Mechanical Engineering, National University of Singapore, Singapore 119260.
[4] Department of Mechanical and Automation Engineering, The Chinese University of Hong Kong, Shatin, NT, Hong Kong.

1 Introduction

Topology optimization is an important design tool for generating more efficient structures. An optimal topology can be obtained by the corresponding modifications of holes and connectivities in the design domain, which is usually implemented by redistributing material as a sizing optimization problem in an iterative and systematic manner [Bendsøe and Kikuchi (1988); Bendsøe and Sigmund (2003); Wang and Tai (2004); Tapp, Hansel, Mittelstedt, and Becker (2004); Wang and Wang (2005, 2004); Wang and Zhou (2004); Wang and Wang (2006); Zhou and Wang (2006); Cisilino (2007); Wang, Lim, Khoo, and Wang (2007b,d,c)]. Topology optimization is one of the most important structural optimization methods because of its ability in achieving largest savings [Rozvany (2001)]. Nevertheless, it is also one of the most challenging tasks in structural design.

The finite element (FE) based continuum topology optimization as a generalized shape optimization problem has experienced tremendous progress since the seminal work of Bendse and Kikuchi [Bendsøe and Kikuchi (1988)] in 1988, as reviewed in detail in [Rozvany (2001)]. Recently, one of the homogenization-based methods, the power-law model or the SIMP (Simple Isotropic Material with Penalization) method [Bendsøe (1989); Rozvany and Zhou (1991); Rozvany, Zhou, and Birker (1992)], has been generally accepted in the field of topology optimization because of its computational efficiency and conceptual simplicity [Rozvany (2001)]. In the SIMP method, the material properties are expressed in terms of the material density using a simple "power-law" interpolation as an explicit means to suppress intermediate values of the bulk density. As shown by Bendse and Sigmund [Bendsøe and Sigmund (1999)], the power-

law interpolation is physically permissible as long as some simple conditions on the power are satisfied. However, like most of the other topology optimization methods, the SIMP method does not directly resolve the problem of non-existence of solutions [Bendsøe and Sigmund (2003)] and thus numerical instabilites, such as the checkerboard instability and mesh-dependency [Bendsøe (1995); Zhou, Shyy, and Thomas (2001); Bendsøe and Sigmund (2003); Wang, Tai, and Quek (2006); Wang and Wang (2005)], may occur. Various approaches have been proposed to overcome these numerical instabilities, including adding slope constraints [Petersson and Sigmund (1998); Zhou, Shyy, and Thomas (2001)] or move limit constraints [Cardoso and Fonseca (2003)] or perimeter controls [Petersson (1999)], using higher order or non-conforming finite elements [Jang, Jeong, Kim, Sheen, Park, and Kim (2003)], and employing filters [Sigmund (1997); Sigmund and Petersson (1998); Bendsøe and Sigmund (1999); Sigmund (2001a); Rozvany (2001); Bendsøe and Sigmund (2003); Wang and Wang (2005)]. Among all these approaches, a filtering technique is the most widely used and has become most popular due to its computational efficiency and ease of implementation [Bendsøe and Sigmund (2003); Sigmund (2007)]. As a numerical method to ensure regularity or existence of solutions to an ill-posed engineering problem, filtering techniques have been quite successful in various domains of engineering applications [Bourdin (2001); Wang and Wang (2005); Wang, Lim, Khoo, and Wang (2007a)].

In the existing filtering techniques for topology optimization, density filtering and sensitivity filtering are the two basic approaches. The density filtering approach was introduced by Bruns and Tortorelli [Bruns and Tortorelli (2001)] and analyzed in detail by Bourdin [Bourdin (2001)]. It was shown that filtering the density can lead to checkerboard-free and mesh-independent designs [Bruns and Tortorelli (2001); Bourdin (2001)]. Nevertheless, this approach may be physically less meaningful [Bendsøe and Sigmund (2003)] due to the introduction of a density measure to replace the bulk density in the original SIMP method. The density filtering approach may also cause a design interpretation problem such as whether the density measure should be used in the volume constraint [Bruns and Tortorelli (2001); Bourdin (2001); Bendsøe and Sigmund (2003); Sigmund (2007)] due to the difference between the bulk density and density measure. The sensitivity filtering approach was first introduced by Sigmund [Sigmund (1994)] and has become much more popular both in academia and in commercial programs [Sigmund (2001a); Bendsøe and Sigmund (2003); Sigmund (2007)]. This filtering approach has been used exclusively in a recent monograph for topology optimization [Bendsøe and Sigmund (2003)]. The main idea of the filtering approach is to use the filtered sensitivities rather than the actual sensitivities to update designs. The filtering sensitivities are made dependent on the sensitivities and densities of the corresponding neighboring elements [Sigmund (1994)], but it can be significantly different from the usual symmetric sensitivity filtering approaches [Sigmund (2007)]. Apparently, this is a heuristic and simple but mathematically less rigorous and potentially risky approach since a filtered sensitivity may not represent a descent direction. However, as stated in [Sigmund (2001a); Bendsøe and Sigmund (2003); Sigmund (2007)], numerous applications have proven the approach to be very robust and reliable using most of the popular optimization tools.

Recently, several researchers have attempted to modify this sensitivity filtering approach to overcome its incapability of producing black-and-white (0-1) designs. Grey regions containing intermediate densities along the solid-void boundary of the final designs can be quite apparent using either the sensitivity or the density filtering approaches [Sigmund (2001a); Bourdin (2001)]. This widely observed phenomenon may cause difficulties in boundary identification and design realization in a post-processing step which is necessary for shape recovery from the optimization solution [Bendsøe and Sigmund (2003); Wang and Wang (2005); Sigmund (2007)]. Furthermore, the topology optimization problem may be inappropriately resolved when the original objective

is to generate distinct solids and voids. To obtain black-and-white designs, a modification for the original sensitivity filtering approach [Sigmund (1994)] was suggested by Borrval [Borrval (2001)]. The density weighting in the denominator is moved inside the summation. Better black-and-white solutions can be obtained, but the checkerboard-free and mesh independence effects of the original sensitivity filtering approach may be destroyed [Sigmund (2007)]. To ensure symmetric behaviour for multi-phase design problems, a sensitivity filtering approach without density filtering was proposed by Sigmund [Sigmund (2001b)]. Due to the elimination of the density weighting, this approach may be unstable and the most desirable filtering effects of the original sensitivity filtering approach may be lost [Sigmund (2007)]. By further dropping the density and distance weightings in the original sensitivity filtering approach, a simplest mean sensitivity filtering approach can be developed [Sigmund (2007)]. Although this approach works well in many cases, it is still unstable and may not generate checkerboard-free and mesh-independent designs. By combining the linear edge smoothing filtering in the spatial domain with the edge preserving smoothing range filtering in the density domain, a bilateral sensitivity filtering approach was proposed by Wang and Wang [Wang and Wang (2005)]. Numerical instabilities can be overcome due to the domain filtering component, while black-and-white designs can be driven due to the range filtering component. However, it would be difficult to choose appropriate filter parameters and resorting to the well-known continuation method [Bendsøe and Sigmund (2003)] may require thousands of iterations, making the approach computationally too expansive. In general, a filtering approach should be simple and easy to implement with fast convergence and low CPU time. Furthermore, the bilateral sensitivity filtering approach may not be robust enough to overcome the numerical instabilities. Due to the existence of these less successful modifications, the original sensitivity filtering approach [Sigmund (1994)] is referred to as the traditional sensitivity filtering approach in the present study. The traditional sensitivity filtering approach has the advantage of overcoming the numerical instabilities robustly to generate checkerboard-free and mesh-independent designs while the modified ones have the advantage of driving the 0-1 convergence to generate black-and-white designs in practice. It is evident that none of the existing sensitivity filtering approaches can be robust and efficient enough to generate checkerboard-free, mesh-independent and black-and-white designs. A sensitivity filtering approach that can incorporate the advantages of the traditional and the modified sensitivity filtering approaches and avoid their drawbacks would be most desirable in topology optimization, but such an approach has not been developed yet.

The objective of the present study is to propose an accurate and efficient hybrid sensitivity filtering approach based on the existing traditional and bilateral sensitivity filtering approaches. In the present approach, the traditional approach is applied only to a sub-domain where the numerical instabilities are likely to occur, while the bilateral approach is employed for the corresponding nearest neighboring elements of mesh-independent holes and there is no filtering for mesh-independent holes. The advantages of both the traditional and the bilateral sensitivity filtering approaches can be inherited while their respective drawbacks can be virtually avoided. The present approach is implemented in the framework of minimum compliance design and its high accuracy and efficiency are illustrated with classical examples.

2 The SIMP Method

The topology optimization problem as a generalized shape optimization problem of finding the optimal material distribution [Rozvany (2001)] is considered. It is confined in a fixed design reference domain, or design domain, $\Omega \in \mathbb{R}^d$ ($d = 2$ or 3) to allow for the applied loads and boundary conditions [Bendsøe and Sigmund (2003)]. The geometric representation of a structure corresponds to a black-and-white raster representation of the geometry with pixels or voxels given by the FE discretization and the material properties are modeled as a function of the discrete density $\overline{\rho}$, $\overline{\rho} \in \{0,1\}$, in which 0 represents void and 1 solid

material. Hence, the original topology optimization problem is a distributed, discrete valued design problem (a 0-1 problem) [Bendsøe and Sigmund (2003)].

In the present study, to simplify the analysis procedure, we only consider the classical minimum compliance topology optimization problem in linear elasticity subject to the applied body force $\boldsymbol{f}$ in Ω and the surface traction forces $\boldsymbol{t}$ on the traction part Γ_t of the smooth boundary $\partial\Omega$, which can be defined as

$$\begin{array}{ll} \min & \ell(\overline{\rho},\boldsymbol{u}) \\ \text{s.t.:} & a_{\overline{\rho}}(\boldsymbol{u},\boldsymbol{v}) = \ell(\overline{\rho},\boldsymbol{v}) \qquad \forall \boldsymbol{v} \in \mathscr{U} \\ & \overline{\rho} \in \{0,1\} \\ & \displaystyle\int_\Omega \overline{\rho}\,\mathrm{d}\Omega = V \leqslant \gamma V_0 \end{array} \tag{1}$$

where

$$\ell(\overline{\rho},\boldsymbol{u}) = \int_\Omega \boldsymbol{f}^T\boldsymbol{u}\,\mathrm{d}\Omega + \int_{\Gamma_t} \boldsymbol{t}^T\boldsymbol{u}\,\mathrm{d}s \tag{2}$$

$$a_{\overline{\rho}}(\boldsymbol{u},\boldsymbol{v}) = \int_\Omega \overline{\rho}\frac{\partial u_i}{\partial x_j} E_{ijkl} \frac{\partial v_k}{\partial x_l}\,\mathrm{d}\Omega \tag{3}$$

and $\boldsymbol{u}$ is the displacement vector that defines the equilibrium of the elastic body, $\boldsymbol{v}$ the kinematically admissible virtual displacement field, $\mathscr{U}$ the set of kinematically admissible displacements, V the allowable volume of solid material ($V > 0$), V_0 the total volume of the fixed reference domain, γ the volume fraction, and E_{ijkl} the elasticity tensor of solid material.

In the design domain Ω, according to the SIMP method in the power-law interpolation of material properties [Bendsøe (1989)], the material properties are modeled as a function of element-wise constant material density ρ, which is a continuous rather than discrete design variable, raised to some power p ($p > 1$) times the material properties of solid material, i.e.,

$$\widetilde{E}(\rho) = \rho^p E \tag{4}$$

where E is the Young's modulus of a given solid material and $\widetilde{E}(\rho)$ the effective Young's modulus. The standard SIMP version of the discrete minimum compliance design problem in Eq. (1) can be expressed as follows:

$$\begin{array}{ll} \min & \ell(\rho,\boldsymbol{u}) \\ \text{s.t.:} & a_\rho(\boldsymbol{u},\boldsymbol{v}) = \ell(\rho,\boldsymbol{v}), \qquad \forall \boldsymbol{v} \in \mathscr{U} \\ & 0 < \rho_{\min} \leqslant \rho \leqslant \rho_{\max} \\ & \displaystyle\int_\Omega \rho\,\mathrm{d}\Omega \leqslant \gamma V_0 \end{array} \tag{5}$$

where

$$\ell(\rho,\boldsymbol{u}) = \int_\Omega \boldsymbol{f}^T\boldsymbol{u}\,\mathrm{d}\Omega + \int_{\Gamma_t} \boldsymbol{t}^T\boldsymbol{u}\,\mathrm{d}s \tag{6}$$

$$a_\rho(\boldsymbol{u},\boldsymbol{v}) = \int_\Omega \rho^p \frac{\partial u_i}{\partial x_j} E_{ijkl} \frac{\partial v_k}{\partial x_l}\,\mathrm{d}\Omega \tag{7}$$

in which $\rho_{\min}$ and $\rho_{\max}$ are the lower and upper limits on the material density ρ, respectively. In this standard SIMP model, the original discrete 0-1 topology optimization problem is converted into a continuous optimization problem with intermediate material densities. As shown by Bendse and Sigmund [Bendsøe and Sigmund (1999)], the power-law interpolation is physically permissible as long as some simple conditions on the power are satisfied.

3 Numerical Implementation

To solve the SIMP version of the minimum compliance topology optimization problem (5) numerically, the finite element method in [Sigmund (2001a)] is used. The design domain Ω is discretized with four-noded bilinear rectangular plane stress elements. The FE discretized design domain Ω can be taken as a digital image and each element a pixel or voxel whose color is represented by its element-wise constant density ρ_e (in a gray scale, white is void and black is solid material). The discrete form of Eq. (5) can be written as

$$\begin{array}{ll} \min & J(\boldsymbol{\rho}) = \mathbf{U}^T\mathbf{K}\mathbf{U} = \displaystyle\sum_{e=1}^{N} (\rho_e)^p\,\mathbf{u}_e^T\mathbf{K}_e\mathbf{u}_e \\ \text{s.t.:} & \displaystyle\sum_{e=1}^{N} (\rho_e)^p\,\mathbf{K}_e\mathbf{u}_e = \mathbf{F} \\ & \displaystyle\sum_{e=1}^{N} \rho_e v_e \leqslant V \\ & 0 < \rho_{\min} \leqslant \rho_e \leqslant \rho_{\max} \quad e = 1,\ldots,N \end{array} \tag{8}$$

where $\boldsymbol{\rho}$ is the design variable vector, $J(\boldsymbol{\rho})$ the objective function (compliance), $\mathbf{U}$ the global displacement vector, $\mathbf{K}$ the global stiffness vector, $\mathbf{u}_e$ and $\mathbf{K}_e$ are the element displacement vector and stiffness matrix (solid element), respectively, ρ_e the unfiltered element density, N the total number of elements used to discretize the reference domain Ω, v_e the element volume, and $\mathbf{F}$ the global force vector.

The sensitivity of the objective function $J(\boldsymbol{\rho})$ can be expressed [Sigmund (2001a); Bourdin (2001); Bendsøe and Sigmund (2003)] as

$$\frac{\partial J}{\partial \rho_i} = -\mathbf{U}^T \frac{\partial \mathbf{K}}{\partial \rho_i}\mathbf{U} = -p\,(\rho_i)^{p-1}\,\mathbf{u}_i^T \mathbf{K}_i \mathbf{u}_i \tag{9}$$

in which the external loads are assumed to be design-independent.

The discretized topology optimization problem described in Eq. (8) can be solved by many approaches such as Optimality Criteria (OC) methods, Sequential Linear Programming (SLP) methods, Sequential Quadratic Programming (SQP), or the Method of Moving Asymptotes (MMA). In the present study, the OC method proposed by Bendse [Bendsøe (1995); Sigmund (2001a); Bendsøe and Sigmund (2003)] is adopted due to its efficiency. As a result, the heuristic updating scheme [Bendsøe (1995)] for the design variable $\boldsymbol{\rho}$ can be formulated as follows:

$$\rho_e^{\text{new}} = \begin{cases} \max(\rho_{\min}, \rho_e - m) & \text{if } \rho_e (B_e)^{\eta} \\ & \leqslant \max(\rho_{\min}, \rho_e - m) \\ \min(\rho_{\max}, \rho_e + m) & \text{if } \rho_e (B_e)^{\eta} \\ & \geqslant \max(\rho_{\max}, \rho_e + m) \\ \rho_e (B_e)^{\eta} & \text{else} \end{cases} \tag{10}$$

where ρ_e^{new} is the updated element density, m a move limit, η a numerical damping coefficient, and B_e can be obtained from the optimality condition [Bendsøe (1995); Sigmund (2001a)], which can be written as

$$B_e = -\frac{\frac{\partial J}{\partial \rho_e}}{\lambda v_e} \tag{11}$$

It should be noted that the descent direction τ_e for the present constrained optimization problem can be given as

$$\tau_e = \frac{\partial J}{\partial \rho_e} + \lambda v_e \tag{12}$$

Nevertheless, with this implementation, significant numerical instabilites, such as checkerboard patterns and mesh-dependent designs, may occur since the SIMP method itself does not directly regularize the well-recognized ill-posed topology optimization problem [Bendsøe and Sigmund (2003)]. The checkerboard instability is mainly due to the inaccuracy of the low-order finite elements and using high-order elements may overcome this problem, as shown in [Jang, Jeong, Kim, Sheen, Park, and Kim (2003)], but the computational cost may become much more expansive. Furthermore, in the SIMP method, the problem of non-existence of optimal solutions is not directly resolved [Bendsøe and Sigmund (2003)] since the naturally posed topology optimization problem is ill-posed and the set of feasible designs is not closed [Bendsøe and Sigmund (2003); Stolpe and Svanberg (2003)]. In order to ensure existence of solutions and mesh-independent designs, one must introduce priori restrictions on the admissible design configurations such as a perimeter constraint, a gradient constraint or with filtering techniques, either globally or locally [Sigmund (2001a); Bendsøe and Sigmund (2003)]. In the present study, a filtering technique is preferred to overcome these numerical instabilities due to its economy and ease of implementation.

4 Traditional Sensitivity Filtering Approach

The sensitivity filtering approaches [Sigmund (1994); Borrval (2001); Sigmund (2001b); Wang and Wang (2005); Sigmund (2007)] use the filtered sensitivity $\frac{\widehat{\partial J}}{\partial \rho_e}$ rather than the unfiltered sensitivity $\frac{\partial J}{\partial \rho_e}$ to update designs in the heuristic density updating scheme (10) of the OC method [Bendsøe (1995)] in hopes of eliminating the significant numerical instabilities. In the traditional sensitivity filtering approach introduced by Sigmund [Sigmund (1994)], the filtered sensitivity

can be written as

$$\frac{\widehat{\partial J}}{\partial \rho_e} = \frac{1}{\rho_e v_e \sum_{i=1}^{N} H_i} \sum_{i=1}^{N} H_i \rho_i v_i \frac{\partial J}{\partial \rho_i} \tag{13}$$

in which the linear hat kernel function H_i can be formulated as

$$H_i = r_{\min} - \mathrm{dist}(e,i),\ \{i \in N \mid \mathrm{dist}(e,i) \leqslant r_{\min}\} \tag{14}$$

where $r_{\min}$ is the filter radius. A theoretically more rigorous expression for the filtered sensitivity, which can be consistent with the continuous filter definition, can be given as

$$\frac{\widehat{\partial J}}{\partial \rho_e} = \frac{v_e}{\rho_e \sum_{i=1}^{N} H_i v_i} \sum_{i=1}^{N} H_i \rho_i \frac{\partial J}{\partial \rho_i} \tag{15}$$

Such a sensitivity filtering approach is apparently heuristic [Bendsøe and Sigmund (2003)]. The topology optimization problem is not well-posed in a rigorous mathematical sense and thus existence of solutions cannot be theoretically proven [Sigmund (2001a)], but numerous applications have shown that the filtering approach produces results very similar to those obtained by other alternative methods and may even generate checkerboard-free and mesh-independent designs in practice with little extra CPU time and implementation effort [Bendsøe and Sigmund (2003)]. Furthermore, the results can be stable under mesh-refinement with a minimum length-scale which is controlled by the filter radius $r_{\min}$. Unfortunately, the theoretical basis behind the success of this approach was little understood or interpreted [Bendsøe and Sigmund (2003); Sigmund (2007)].

According to Eq. (9), the terms to be filtered in the numerator in Eq. (13) can be written as follows:

$$\mathscr{J}_i = \rho_i v_i \frac{\partial J}{\partial \rho_i} = -p\, v_i (\rho_i)^p \mathbf{u}_i^T \mathbf{K}_i \mathbf{u}_i = -p\, U_i \tag{16}$$

where U_i is the element strain energy given by

$$U_i = v_i (\rho_i)^p \mathbf{u}_i^T \mathbf{K}_i \mathbf{u}_i \tag{17}$$

Hence, the filtered sensitivity $\frac{\widehat{\partial J}}{\partial \rho_e}$ in Eq. (13) can be rewritten as

$$\frac{\widehat{\partial J}}{\partial \rho_e} = \frac{-p}{\rho_e v_e \sum_{i=1}^{N} H_i} \sum_{i=1}^{N} H_i U_i \tag{18}$$

Therefore, it is the spatial distribution of the element strain energy that is filtered in the traditional sensitivity filtering approach. The traditional sensitivity filter shown in Eq. (13) or (18) is actually a non-standard and unsymmetric sensitivity filter and can be quite different from the symmetric sensitivity filters in the literature [Borrval (2001); Sigmund (2001b); Wang and Wang (2005); Sigmund (2007)]. As a result, the traditional sensitivity filtering approach can be robust enough to delay the tendency of overly fast 0-1 convergence to produce checkerboard-free and mesh-independent designs.

Patches of checkerboard patterns are often seen in final designs using the SIMP topology optimization method together with a low-order displacement based finite element method, as aforementioned. Within a checkerboard pattern, the material density assigned to contiguous finite elements varies in a periodic fashion similar to a checkerboard consisting of alternating solid and void elements [Bendsøe and Sigmund (2003)]. It has been well understood that the checkerboard instability is due to the inaccuracy of low-order quadrilateral finite elements in estimating the stiffness of a checkerboard pattern [Bendsøe and Sigmund (2003)]. As aforementioned, a filtering technique would be more competitive in terms of the computational cost than using higher-order finite elements or non-conforming finite elements [Jang, Jeong, Kim, Sheen, Park, and Kim (2003)] to eliminate the checkerboard patterns. Furthermore, it is well-known that the SIMP method topology optimization problem is ill-posed in its general continuum setting [Bendsøe (1995); Bendsøe and Sigmund (2003)] and thus existence of solutions cannot be guaranteed. Theoretically, the introduction of more holes without changing the structural volume may increase the efficiency of a given structure [Bendsøe and Sigmund (2003)] and thus the final optimum may even include infinitesimal holes [Michell (1904); Eschenauer and Olhoff (2001)]. In computational implementations, this effect is demonstrated by mesh-dependent designs, in which the size of the minimum holes is dependent of the mesh size. This dependency is also regarded as a numerical

instability since a large number of smaller holes may be generated when a finer finite element mesh is adopted. As aforementioned, a filtering technique can also be employed to produce mesh-independent designs to eliminate this numerical instability [Bendsøe and Sigmund (2003)].

To produce a checkerboard pattern, the local densities in a filter window defined by the filter radius must be significantly different and similar to a checkerboard pattern. This difference may be further enlarged in the element strain energy distribution due to the power-law model of the SIMP method [Bendsøe (1989)]. The filtered strain energy can be written as

$$\widehat{U}_e = \frac{\sum_{i=1}^{Ns} H_i U_i}{\sum_{i=1}^{Ns} H_i} \tag{19}$$

where Ns is the total number of elements in the filter window. As a result, the element strain energy distribution is smoothed. The elements with low density will be given a higher strain energy while those with high density will be given a lower strain energy. According to Eq. (18), the filtered sensitivity $\frac{\widehat{\partial J}}{\partial \rho_e}$ can be re-written as

$$\frac{\widehat{\partial J}}{\partial \rho_e} = -\frac{p\widehat{U}_e}{\rho_e v_e} \tag{20}$$

Hence, the filtered sensitivity of a low-density element will become higher and the filtered sensitivity of a high-density element will become lower. The tendency of 0-1 convergence of these elements will be delayed, according to the density updating scheme (10) of the OC method [Bendsøe (1995)]. The occurrence of checkerboard patterns can thus be prevented. Especially, if a checkerboard pattern has been generated, according to Eq. (20), the filtered sensitivity of a void element would become sufficiently large such that the decent direction as shown in Eq. (12) will be changed. The void elements will thus become non-void, according to the density updating scheme (10) of the OC method [Bendsøe (1995)]. Hence, the traditional sensitivity filter is robust enough to eliminate the checkerboard patterns. Similarly, it can be obtained that the traditional sensitivity filter is also robust enough to eliminated the mesh-dependent small holes (smaller than the size defined by the filter radius) to produce mesh-independent designs. It should be noted that the density ρ_e in the denominator of the traditional sensitivity filter (13) plays a crucial role in overcoming these numerical instabilities.

Other sensitivity filtering approaches [Borrval (2001); Sigmund (2001b); Wang and Wang (2005); Sigmund (2007)] may fail to generate checkerboard-free and mesh-independent designs due to their inefficiency to delay the tendency of 0-1 convergence or to change the decent direction. For example, the modified sensitivity filter suggested by Borrvall [Borrval (2001)] as

$$\frac{\widehat{\partial J}}{\partial \rho_e} = \frac{1}{\sum_{i=1}^{N} H_i \rho_i v_i} \sum_{i=1}^{N} H_i \rho_i v_i \frac{\partial J}{\partial \rho_i} \tag{21}$$

cannot guarantee that the filtered sensitivity of a void element in a checkerboard pattern be sufficiently large due to the fact that the filtered sensitivity is only a weighted average of sensitivities of neighboring elements. Since the decent direction of this void element may not be changed, the checkerboard pattern cannot be eliminated. Hence, the modified sensitivity filter is neither robust nor sufficient to overcome the checkerboard instability, though it has the advantage of generating designs with better 0-1 convergence [Sigmund (2007)].

Nevertheless, the side effects of this traditional sensitivity filtering approach may be quite undesirable in the SIMP topology optimization, though its merits in producing checkerboard-free and mesh-independent designs are prominent. The most evident side effect is the blurry boundaries of the mesh-independent holes since the sensitivity filter Eq. (13) blurs not only the mesh-independent relatively small holes but also the mesh-independent relatively large holes. This filtering effect on mesh-independent holes is quite undesirable in general since the 0-1 convergence driven by the power-law penalization of the SIMP method on intermediate densities [Bendsøe (1995); Bendsøe and Sigmund (1999, 2003)] is seriously hampered and to obtain black-and-white designs would become impossible. Furthermore, the material in the blurry transition regions would be quite ineffectively used and sub-optimal solu-

tions may thus be generated. Since the element strain energy is naturally discontinuous at the boundary of a mesh-independent hole, employing a filter to smooth out this reasonable discontinuity would become physically meaningless. The minimum length-scale constraint [Bendsøe and Sigmund (2003); Sigmund (2007)] on structural members imposed by the traditional sensitivity filter may also be undesirable. Since the actual manufacturing constraint may be with high precision, this rough minimum length-scale due to the blurry boundary may be not desirable. More importantly, incorporating a minimum length-scale constraint on structural members into topology optimization is unnecessary and risky since topology optimization as a conceptual design tool should only concentrate on the size-irrelevant geometry while the minimum member size constraint can be more effectively and appropriately handled by sizing optimization [Bendsøe and Sigmund (2003)]. This minimum length-scale constraint may even be destructive to topology optimization since the underlying topology may be changed due to the possible elimination of relatively small structural members.

5 Bilateral Sensitivity Filtering Approach

In the bilateral sensitivity filtering approach proposed by Wang and Wang [Wang and Wang (2005)], the filtered sensitivity can be written as

$$\frac{\widehat{\partial J}}{\partial \rho_e} = k^{-1}(e) \sum_{i=1}^{N} D_i S_i v_i \frac{\partial J}{\partial \rho_i} \tag{22}$$

where

$$k(e) = \sum_{i=1}^{N} D_i S_i v_i \tag{23}$$

$$D_i = e^{-\frac{1}{2}(\mathrm{dist}(e,i))^2/{\sigma_d}^2} \tag{24}$$

$$S_i = e^{-\frac{1}{2}{\Delta_i}^2/{\sigma_r}^2} \tag{25}$$

$$\Delta_i = \frac{\partial J}{\partial \rho_i} - \frac{\partial J}{\partial \rho_e} \tag{26}$$

in which σ_d and σ_r are the geometric spread and photometric spread [Tomasi and Manduchi (1998)], respectively. It can be seen that the bilateral filter combines a domain filter component D_i in the spatial domain with a range filter component S_i in the sensitivity domain. As a result, the filtered sensitivity is an average of similar and nearby sensitivity values.

The bilateral sensitivity filter shown in Eq. (22) is a nonlinear edge preserving smoothing filter [Tomasi and Manduchi (1998)], which may result in a significant advantage over other types of filters [Sigmund (1994); Bruns and Tortorelli (2001); Borrval (2001); Sigmund (2001b)] in generating black-and-white designs due to its range filter component. In bilateral filtering, the crisp edges or boundaries can be preserved during smoothing [Tomasi and Manduchi (1998); Durand and Dorsey (2002); Elad (2002); Jiang, Baker, Wu, Bajaj, and Chiua (2003); Fleishman, Drori, and Cohen (2003); Zhou, Hu, and He (2004)]. Since the range filter component S_i only affects similar sensitivity values, the weights for the neighboring pixels are almost zero if the center pixel is at the edge and averaging across edges while smoothing an image is thus prevented [Wang and Wang (2005)].

In the bilateral sensitivity filter, a larger geometric spread σ_d or photometric spread σ_r may cause more severe smoothing [Tomasi and Manduchi (1998); Wang and Wang (2005)]. The bilateral filtering may be similar to the normal low pass filter for a too large photometric spread σ_r. Furthermore, no filtering will be introduced for a too small σ_r or σ_d. When σ_r is infinite, the bilateral filter is reduced to a normal low pass filter [Jiang, Baker, Wu, Bajaj, and Chiua (2003)]. Therefore, appropriate choice of these two filter parameters for the bilateral sensitivity filter is required to overcome the numerical instabilities while preserving the boundaries of mesh-independent holes to favor the 0-1 convergence. The well-known continuation method [Petersson and Sigmund (1998); Bendsøe and Sigmund (2003)] can be used to reduce the dependence on the filter parameters to achieve checkerboard-free, mesh-independent and black-and-white designs. However, the computational cost would be expansive in terms of the number of iterations and CPU time. Furthermore, there is no guarantee that checkerboard-free, mesh-independent and black-

and-white designs be finally and fully generated. The bilateral sensitivity filtering approach cannot be robust enough to eliminate a given checkerboard pattern due to the fact that the filtered sensitivity of a void element would not be sufficiently large to change the decent direction, as aforementioned. Therefore, further improvements over the bilateral sensitivity filtering approach for the SIMP method topology optimization are needed.

6 Present Hybrid Sensitivity Filtering Approach

In the present approach, the traditional sensitivity filtering approach is combined with the bilateral sensitivity filtering approach such that their respective merits can be inherited while their drawbacks can be avoided. The basic idea is that the traditional sensitivity filter is confined in a subdomain where numerical instabilities are likely to occur while the bilateral sensitivity filter is employed for the corresponding nearest neighboring elements of mesh-independent holes and no filtering is introduced for mesh-independent holes during the iterations of the optimization procedure. The theoretical basis is that the numerical instabilities demonstrated as checkerboard patterns and mesh-dependent holes are only a local phenomenon so that the priori restrictions on the admissible design configurations such as a perimeter, gradient, or filtering constraint can be introduced either globally or locally [Sigmund (2001a); Bendsøe and Sigmund (2003)], as aforementioned. Apparently, if the numerical instabilities were not a local phenomenon, the traditional sensitivity filtering approach would not have become so successful since the global change of the decent directions imposed by the traditional sensitivity filter to overcome the numerical instabilites would have made the objective function increase and the topology optimization problem would have been inappropriately resolved in general. It should be noted that it is impossible to cause the numerical instabilities inside mesh-independent holes after updating the densities using the heuristic density updating scheme [Bendsøe (1995)] as shown in Eq. (10).

The filtered sensitivity $\frac{\widehat{\partial J}}{\partial \rho_e}$ of the present hybrid sensitivity filtering approach can be written as

$$\frac{\widehat{\partial J}}{\partial \rho_e} = \begin{cases} \dfrac{1}{\rho_e v_e \sum_{i=1}^{N} H_i} \sum_{i=1}^{N} H_i \rho_i v_i \dfrac{\partial J}{\partial \rho_i}, & e \in \Omega_t \\ k^{-1}(e) \sum_{i=1}^{N} D_i S_i v_i \dfrac{\partial J}{\partial \rho_i}, & e \in \Omega_b \\ \dfrac{\partial J}{\partial \rho_e}, & e \in \Omega_n \end{cases} \tag{27}$$

where

$$\Omega_f \cup \Omega_b \cup \Omega_n = \Omega \tag{28}$$

$$\Omega_f \cap \Omega_n = \emptyset, \quad \Omega_f \cap \Omega_b = \emptyset, \quad \Omega_b \cap \Omega_n = \emptyset \tag{29}$$

The traditional sensitivity filter (13) is only applied to the sub-domain Ω_t in which the traditional sensitivity filtering is desirable to overcome the numerical instabilities robustly, the bilateral sensitivity filter is limited to the sub-domain Ω_b defined by the nearest neighboring elements of mesh-independent holes where 0-1 convergence is most desirable, and no filtering is introduced to the sub-domain Ω_n defined by the mesh-independent holes in which sensitivity filtering is undesirable and unnecessary to save the computational cost. In this study, Ω_n and Ω_b are to be explicitly defined using an image-processing-based technique and Ω_t can be subsequently obtained from Eqs. (28) and (29).

In order to define the non-filtering sub-domain Ω_n and the bilateral sensitivity filtering sub-domain Ω_b explicitly, some image-processing techniques have to be introduced to identify holes in the design domain Ω. In image processing for a 2D problem, either a 4-neighborhood connectivity, where only vertical and horizontal directions can be followed, or a 8-neighborhood connectivity, where horizontal, vertical and diagonal directions are allowed, can be used [Jahne (1997); Wang, Lim, Khoo, and Wang (2007b)], as shown in Fig. 1. To determine the structural connectivity more effectively, the 4-neighborhood connectivity measure as shown in Fig. 1(a) is employed in the present study since the undesirable patches of checkerboard patterns will not be considered as appropriately connected due to its edge connection requirement [Wang and Tai (2005b);

Wang, Tai, and Wang (2006)]. Moreover, the connected components labeling approach [Jahne (1997); Chang, Chen, and Lu (2004)] in image processing is also used for the present hole identification. The connected components labeling approach scans an image and groups its pixels into components based on pixel connectivity. Once all groups have been determined, each pixel is labeled with a unique (integer) number according to the component it was assigned to. With this labeling, the number of connected regions and their relative areas can be readily obtained with a simple inspection of the labeled image's histogram [Wang and Tai (2005b); Wang and Wang (2005)]. The connected components labeling approach can work on binary or gray-level images and different measures of connectivity. In the present analysis, a design is to be further taken as a binary image for hole identification. The connected components labeling approach based on the binary image and 4-neighborhood connectivity measure can then be used to identify mesh-independent holes of a design to define the sub-domains Ω_n and Ω_b.

To carry out hole identification to obtain mesh-independent holes of a design, a hole definition must be first given. In the present study, a hole of a 2D FE-discretized design is defined as a group of connected void elements whose densities are exactly $\rho_{\min}$ using the 4-neighborhood connectivity measure. Based on this hole definition, a design usually taken as a gray-level image [Bendsøe and Sigmund (2003)] can be converted into a work binary image for the connected components labeling approach. Figure 2 displays the conversion process. The binary image in Fig. 2(b) is converted from the gray-level image in Fig. 2(a) by assuming that

$$\rho_e = \begin{cases} 0, & \text{if } \rho_e = \rho_{\min} \\ 1, & \text{if } \rho_{\min} < \rho_e \leqslant \rho_{\max} \end{cases} \tag{30}$$

and the work image shown in Fig. 2(c) is obtained by performing a NOT (inverter) Boolean logic operation on the binary image in Fig. 2(b). It should be noted that the connected void elements depicted in black at the boundary of the design domain Ω in Fig. 2(c) are also considered as holes for the sake of simplicity. Based on this work binary image, the connected components labeling approach can be used to obtain the number of holes and their sizes to further identify mesh-independent and so-called nascent holes. In this study, a nascent hole indicates a hole whose size is smaller than the size defined by the filter radius $r_{\min}$ but the nearest neighboring elements are with intermediate densities, implying that the hole is at the nascent stage to become a distinct hole. The identification of nascent holes with blurry boundaries is necessary to drive 0-1 convergence at the boundaries of these holes such that the minimum length-scale constraint controlled by the filter radius can be accurately imposed. This constraint on the minimum hole size is crucial to achieve well-posedness of the optimization problem and ensure existence of solutions [Bendsøe and Sigmund (2003)]. The traditional sensitivity filtering approach cannot guarantee that the minimum hole size constraint be satisfied rigorously due to the blurry boundaries of all of the holes. If the nearest neighboring elements are solid, the hole should be regarded as a mesh-dependent hole and the traditional sensitivity filter should be applied to smooth out the hole and overcome the numerical instability .

The sub-domains Ω_n and Ω_b can be readily defined after identifying the mesh-independent and nascent holes for a design during the optimization process. Figure 3 shows the definitions of the bilateral sensitivity filtering and non-filtering regions for the mesh-independent and nascent holes. An identified mesh-independent or nascent hole is defined as a non-filtering region in black color while its nearest neighboring elements a bilateral sensitivity filtering region in grey color. The non-filtering sub-domain Ω_n can be expressed as

$$\Omega_n = \bigcup_{i=1}^{N^h} \mathscr{A}_i \tag{31}$$

where N^h is the total number of the mesh-independent and nascent holes, and $\mathscr{A}_i$ the non-filtering region of the i-th hole. Since filtering is disabled in Ω_n, the destructive minimum length-scale constraint on the sizes of structural mem-

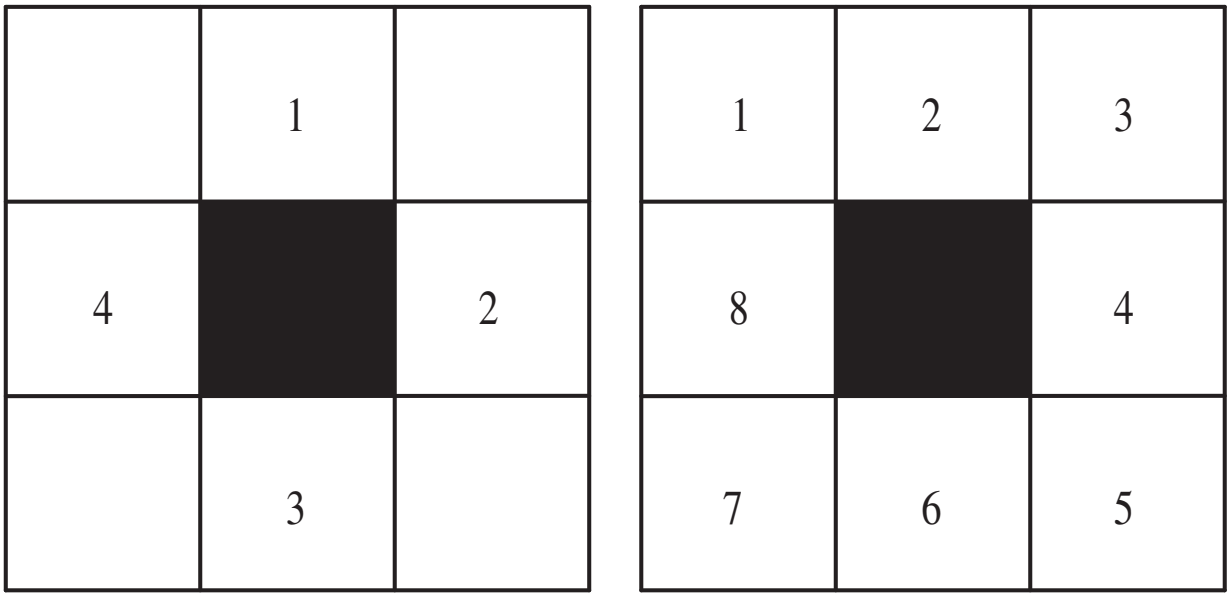

(a) 4-neighborhood connectivity (b) 8-neighborhood connectivity

Figure 1: Connectivity measures for a 2D problem.

bers between the mesh-independent holes is also disabled and thus the present approach can avoid the risk of converging to a sub-optimal solution due to the possible elimination of structural members imposed by the minimum member size constraint. Similarly, the bilateral sensitivity filtering sub-domain Ω_b can be expressed as

$$\Omega_b = \bigcup_{i=1}^{N^h} \mathscr{B}_i \tag{32}$$

where $\mathscr{B}_i$ is the bilateral sensitivity filtering region of the i-th mesh-independent or nascent hole. According to the present definitions, we have

$$\mathscr{A}_i \cap \mathscr{B}_i = \emptyset, \quad \Omega_n \cap \Omega_b = \emptyset \tag{33}$$

and thus the traditional sensitivity filtering sub-domain Ω_t can be readily obtained, according to Eqs. (28) and (29).

In the bilateral sensitivity filtering sub-domain Ω_b, checkerboard-patterns and mesh-dependent holes are unlikely to occur due to the present definition of each bilateral sensitivity filtering region round a hole. Since the bilateral filter has a range filter component to preserve the significant differences inside the filter window, the tendency of 0-1 convergence driven by the power-law penalization on intermediate densities in the SIMP method [Bendsøe (1989); Rozvany (2001); Bendsøe and Sigmund (2003)] can also be preserved. Hence, distinct boundaries of mesh-independent holes can be produced in the final designs in general. In the traditional sensitivity filtering sub-domain Ω_t, patches of checkerboard-patterns and mesh-dependent holes can be suppressed robustly due to the traditional sensitivity filter. However, 0-1 convergence cannot be guaranteed due to the apparent delay on the tendency of 0-1 convergence imposed by the traditional sensitivity filter, as aforementioned. The transition regions with intermediate densities, which can be taken as an indication of blurred mesh-dependent holes, may appear in the final designs, depending on the filter radius and mesh size. Therefore, the final designs maybe mostly black-and-white, rather than complete black-and-white. Since the sizes of the blurred mesh-dependent holes are smaller than the size defined by the filter radius, the existence of these transition regions can be reasonable and should not affect the optimal topologies, which may be represented by the dis-

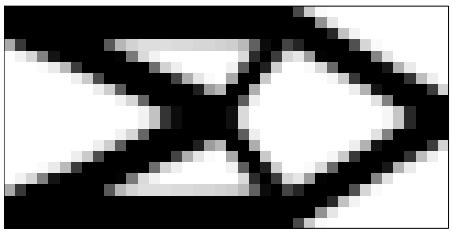

(a) Gray-level image

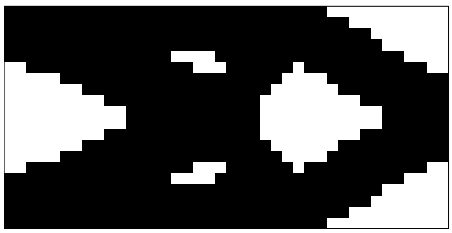

(b) Binary image conversion

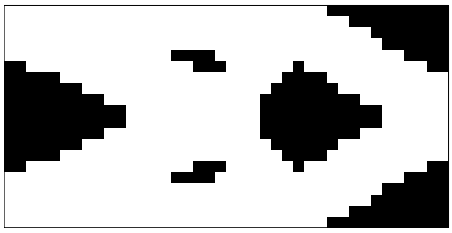

(c) Work image conversion

Figure 2: Image conversion of a design for hole identification.

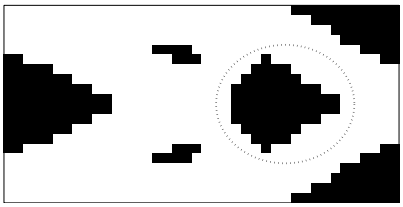

(a) A mesh-independent hole

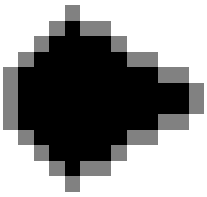

(b) Filtering (grey) and non-filtering (black) regions for the mesh-independent hole

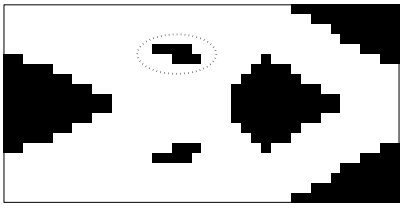

(c) A nascent hole

(d) Filtering (grey) and non-filtering (black) regions for the nascent hole

Figure 3: Definition of the bilateral sensitivity filtering and non-filtering regions.

tinct mesh-independent holes. Furthermore, the present mostly black-and-white designs may not pose difficulties in boundary identification and design realization in practice due to the distinct boundaries of mesh-independent holes. Hence, complete black-and-white designs may be unnecessary in topology optimization. Nevertheless, if complete black-and-white designs are of the major concern, a relatively large filter radius should be used to prevent the occurrence of the transition regions, or the well-recognized continuation method [Bendsøe and Sigmund (2003)] should be employed to gradually remove those transition regions in the traditional sensitivity filtering subdomain Ω_t. The former is computationally efficient, but the objective function value may be worse since the optimal topology may become simpler. The latter may not cause further topological changes, but it is computationally expansive and 0-1 convergence cannot be guaranteed.

As a whole, the present hybrid sensitivity filtering approach combines the traditional sensitivity filter to overcome the numerical instabilities with the bilateral sensitivity filter to favor the occurrence of distinct boundaries of mesh-independent holes. As a result, the numerical instabilities can be effectively and robustly suppressed and distinct boundaries of mesh-independent holes can

be achieved. Existence of solutions can be ensured more accurately and the side effects of both the traditional and the bilateral sensitivity filters can be avoided or alleviated. The present approach can achieve not only checkerboard-free and mesh-independent but also mostly black-and-white designs. Furthermore, as illustrated in the present numerical examples, the present approach is computationally at least as efficient as the traditional sensitivity approach since the present image-processing-based hole identification technique is simple to implement and filtering is prohibited in the non-filtering sub-domain Ω_n, which is usually large in topology optimization [Rozvany (2001)]. Therefore, the present approach can be both accurate and efficient for the SIMP method topology optimization.

7 Examples and Discussion

Classical examples are used to demonstrate both the accuracy and efficiency of the present hybrid sensitivity filtering approach for topology optimization. Unless otherwise stated, all the units are consistent and the following parameters are assumed as: $\rho_{\min} = 0.001$, $\rho_{\max} = 1$, Young's modulus $E = 1$, Poisson's ratio $\nu = 0.3$, power $p = 3$, move limit $m = 0.2$, damping coefficient $\eta = 0.5$, geometric spread $\sigma_d = r_{\min}/2$, and photometric spread $\sigma_r = 0.1$. The present algorithm is based on an initial design in which each element has the same density as the volume fraction and terminated when the relative difference between two successive objective function values is less than 10^{-6} or a prescribed maximum number of iterations has been reached. The FE analysis is based on the bilinear rectangular elements in [Sigmund (2001a)] and all the comparisons on the objective function values are based on the final results when the iteration is terminated. All the CPU time is based on a desktop computer under the MATLAB environment with two Intel Pentium IV processors of 3.0 GHz clock speed.

7.1 A Two-bar Problem

The classical two-bar topology optimization problem for which the optimal solution has been obtained analytically [Michell (1904)] is used for the verification of the present approach and demonstration of its efficiency. The clamped deep beam with a fixed 10×24 rectangular design domain as shown in Fig. 4 is adopted as a minimum compliance design problem, which has been studied by many other researchers such as Xie and Steven [Xie and Steven (1993)], Bulman et al. [Bulman, Sienz, and Hinton (2001)], Wang and Tai [Wang and Tai (2005a)], and Wang and Wang [Wang and Wang (2005)]. The beam is fully clamped along the left-hand edge and a load P is applied at the centre of the right-hand edge. The design domain is discretized with a regular FE mesh. The basic parameters are assumed to be: thickness $t = 1.0$, load $P = 1$ and the volume fraction $\gamma = 0.20$ [Bulman, Sienz, and Hinton (2001)]. The analytical solution for this problem is known to be a two-bar structure with an internal angle of 90° [Xie and Steven (1993); Bulman, Sienz, and Hinton (2001)]. For the purpose of comparison, the solution provided by the homogenization-based method (CATO-mc) [Bulman, Sienz, and Hinton (2001)] is also depicted in Fig. 4. It can be seen that the solution is similar to a two-bar structure with an internal angle of 90°, but the homogenization-based method may produce a final design with grey elements at the boundary and is thus less desirable.

Figure 5 shows the optimal topologies for the two-bar problem using the traditional sensitivity filtering approach with a filter radius of $r_{\min} = 0.48$ and four different meshes. It can be seen that the traditional approach can achieve checkerboard-free and mesh-independent designs similar to the analytical two-bar solution, but cannot produce distinct black-and-white designs due to the blurry boundary. Figure 6 shows the optimal topologies using the bilateral sensitivity filtering approach. It can be seen that the bilateral approach may achieve black-and-white designs, but may preserve the numerical instability shown as mesh-dependent holes at the fixed end of the designs.

Figure 7 shows the the optimal topologies using the present hybrid sensitivity filtering approach. The optimal topologies achieved by the present approach are also similar to the analytical solution and can also be checkerboard-free and mesh-

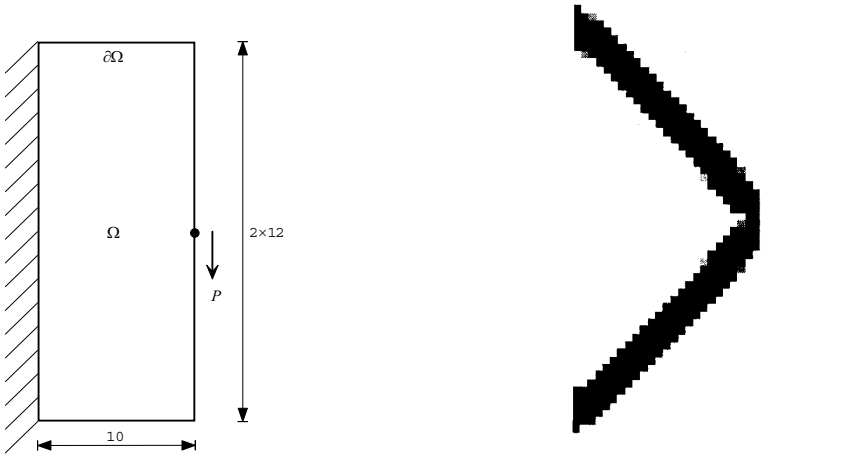

(a) Problem definition (b) Solution by a homogenization method

Figure 4: A two-bar topology topology optimization problem.

independent as the traditional approach. More importantly, as shown in Fig. 7, black-and-white designs can be obtained. Hence, the present approach is an excellent combination of the traditional and the bilateral sensitivity filtering approaches. The distinct boundaries are zigzag due to the element-wise constant density assumption and thus the boundary-based shape optimization [Bendsøe and Sigmund (2003)] may be needed to obtain a smooth shape. It can also be seen that the zigzag boundaries become much smoother when finer finite element meshes are used, however, the computational cost may become much more expansive.

A further comparison on the accuracy and efficiency is listed in Table 1. It can be seen that the traditional sensitivity filtering approach may only achieve an infeasible and sub-optimal solution in terms of the 0-1 convergence measured by the average density ρ^* of all the non-void elements [Wang and Wang (2005)] and the final minimum compliance $J_{\min}$, while the bilateral approach may achieve a feasible but sub-optimal solution. The present approach can achieve a feasible and optimal solution due to its combination of the first two approaches. It can also be seen that the present approach can be as efficient as, or more efficient than, the traditional approach. The bilateral approach is the most inefficient one due to its computational complexities as shown in Eq. (22). Table 1 also shows that the CPU time is not dominated by the sensitivity filtering since the fraction of CPU time on filtering is little, especially when a fine mesh is used. Hence, using filtering approaches to overcome the numerical instabilities are economical in general. Figure 8 shows the convergence history of the objective function using the present approach. It can be seen the convergence is quite stable for the four different meshes. Since the numerical instabilities are only a local phenomenon, the decent directions can only be changed locally by the present hybrid sensitivity filter, the decrease of the objective function can thus be unaffected.

7.2 Short Cantilever Beam

A short cantilever beam minimum compliance design problem defined in a fixed $L \times H$ rectangular design domain as illustrated in Fig. 9 is considered. The basic parameters are assumed to be $L = 2$, $H = 1$, thickness $t = 1.0$, load $P = 1$ and a volume fraction of 0.5. Figure 10 displays the optimal topologies using the traditional sensitivity filtering approach with a filter radius of $r_{\min} = 0.06$ and four different meshes. Again, it illustrates that the traditional approach produces checkerboard-free and mesh-independent designs with relatively poor 0-1 convergence at the bound-

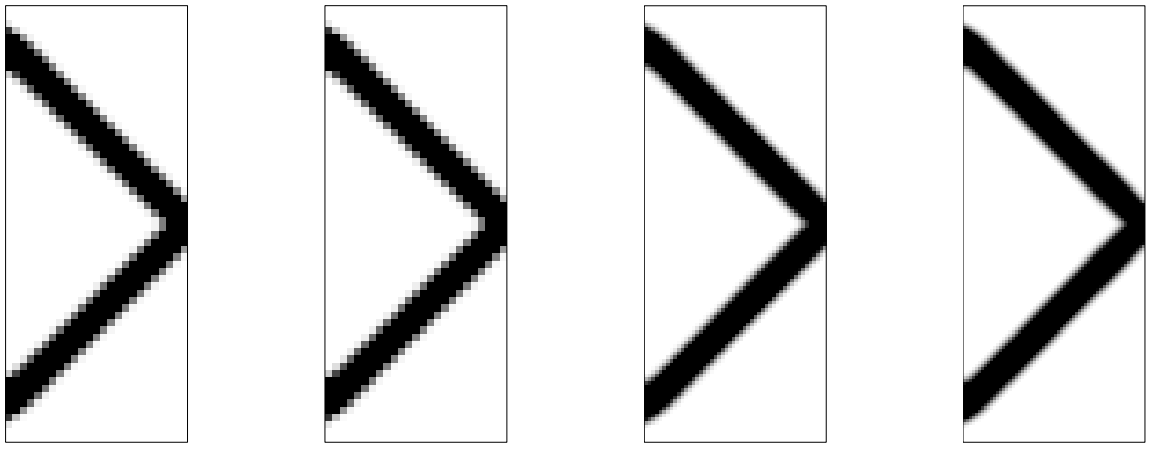

(a) Mesh 25×60 (b) Mesh 40×96 (c) Mesh 50×120 (d) Mesh 60×144

Figure 5: Optimal topologies for the two-bar problem using the traditional sensitivity filtering method.

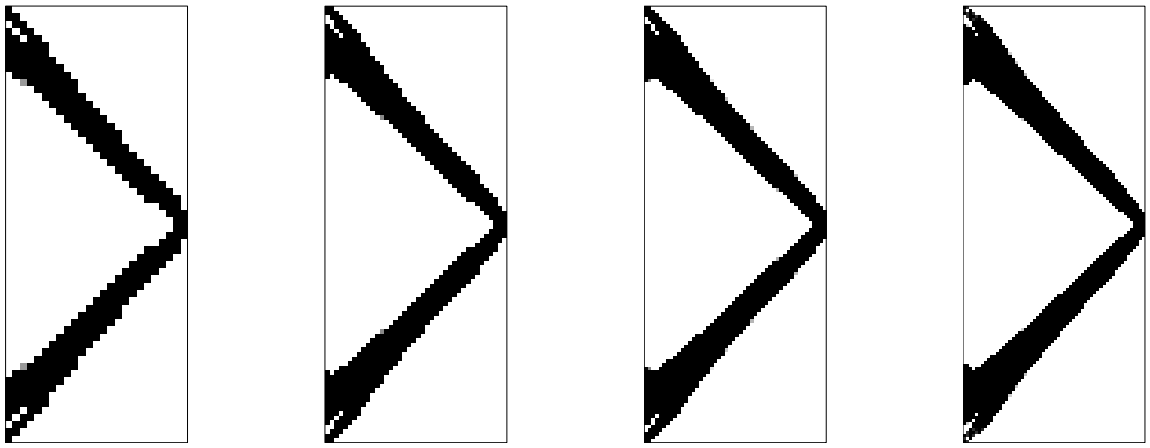

(a) Mesh 25×60 (b) Mesh 40×96 (c) Mesh 50×120 (d) Mesh 60×144

Figure 6: Optimal topologies for the two-bar problem using the bilateral sensitivity filtering method.

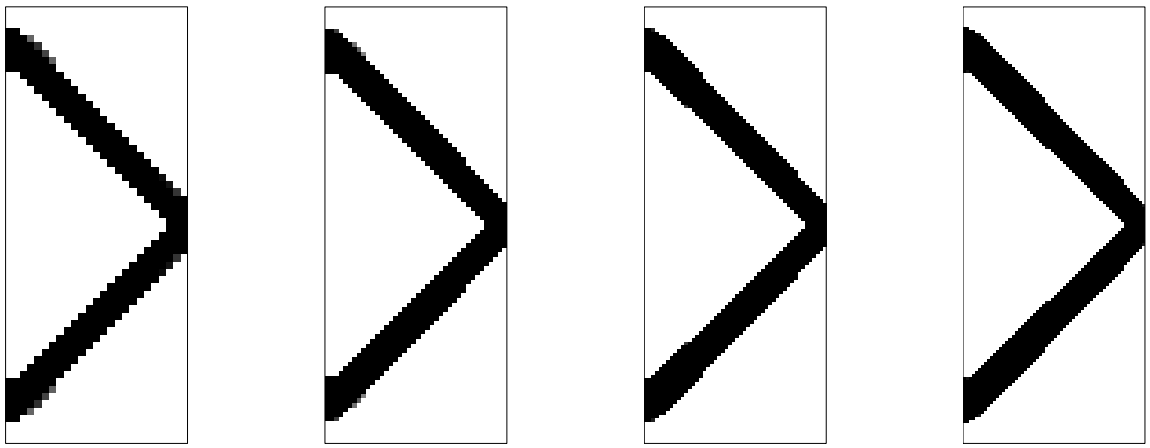

(a) Mesh 25×60 (b) Mesh 40×96 (c) Mesh 50×120 (d) Mesh 60×144

Figure 7: Optimal topologies for the two-bar problem using the present hybrid sensitivity filtering approach.

Table 1: Solutions to the two-bar problem using different sensitivity filtering approaches.
($\overline{t}_{\rm it}$: average CPU time per iteration; $\overline{t}_{\rm fil}$: average CPU time on filtering per iteration; $\overline{t}_{\rm frac} = \overline{t}_{\rm fil}/\overline{t}_{\rm it}$)

Mesh	Approach	$J_{\min}$	ρ^*	Iterations	$\overline{t}_{\rm it}$	$\overline{t}_{\rm fil}$	$\overline{t}_{\rm frac}$
25×60	Traditional	10.347	0.695	56	0.976	0.075	0.0772
	Bilateral	10.092	0.996	21	0.952	0.112	0.1180
	Hybrid	9.390	0.964	94	0.894	0.078	0.0872
40×96	Traditional	10.473	0.668	100	3.817	0.190	0.0497
	Bilateral	10.338	0.999	100	3.946	0.260	0.0658
	Hybrid	9.541	0.993	83	3.906	0.196	0.0501
50×120	Traditional	10.678	0.647	100	8.481	0.341	0.0403
	Bilateral	10.430	0.993	28	8.178	0.561	0.0686
	Hybrid	9.678	0.999	48	8.147	0.313	0.0384
60×144	Traditional	10.763	0.664	100	15.287	0.501	0.0328
	Bilateral	10.664	0.994	100	17.889	0.797	0.0446
	Hybrid	9.778	0.998	35	15.341	0.456	0.0297

aries. Figure 11 shows the optimal topologies using the bilateral sensitivity filtering approach. Again, it shows that the bilateral approach (using the given photometric spread $\sigma_r = 0.1$) produces black-and-white designs, but preserves the significant numerical instabilities.

Figure 12 shows the optimal topologies generated by the present hybrid sensitivity filtering approach. The ability of present approach in achieving checkerboard-free, mesh-independent and black-and-white designs is again demonstrated. Table 2 displays a comparison on the efficiency and accuracy between different sensitivity filtering approaches. Again, it can be seen that the present approach can be more accurate and efficient than the traditional or bilateral approach and the sensitivity filtering itself is computationally efficient due to the little extra CPU time.

7.3 2D Bridge

A 2D bridge minimum compliance design problem defined in a fixed $L\times H$ rectangular design domain as illustrated in Fig. 13 is investigated. The basic parameters are assumed to be: $L = 2$, $H = 1.2$, thickness $t = 1.0$, load $P = 1$ and a volume fraction of 0.4. Figure 14 displays the optimal topologies generated by the traditional sensitivity filtering approach with a filter radius of

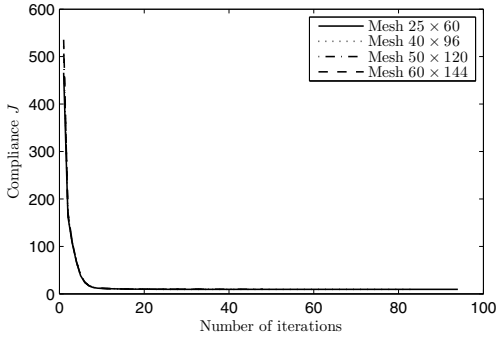

Figure 8: Convergence history of the compliance for the two-bar problem using the present approach.

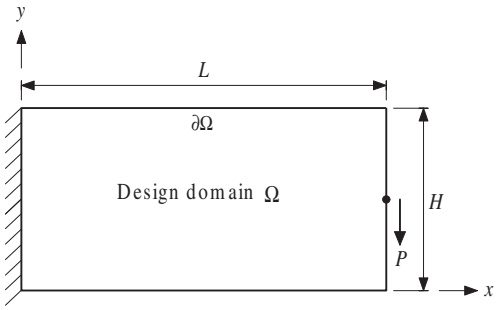

Figure 9: A short cantilever beam problem.

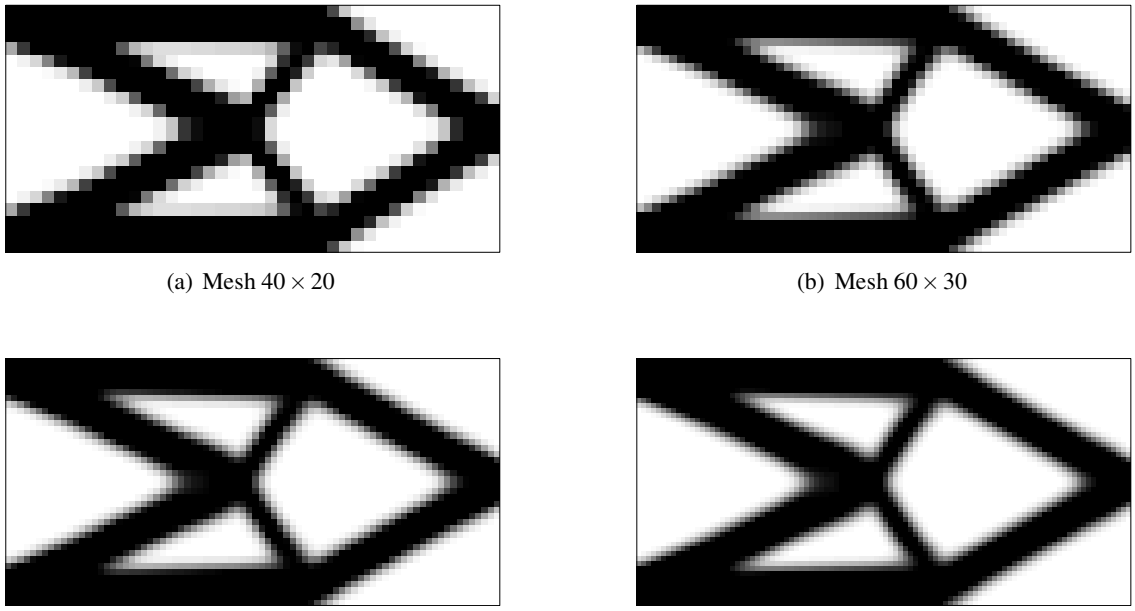

(a) Mesh 40×20 (b) Mesh 60×30

(c) Mesh 80×40 (d) Mesh 100×50

Figure 10: Optimal topologies for the short cantilever problem using the traditional sensitivity filtering method.

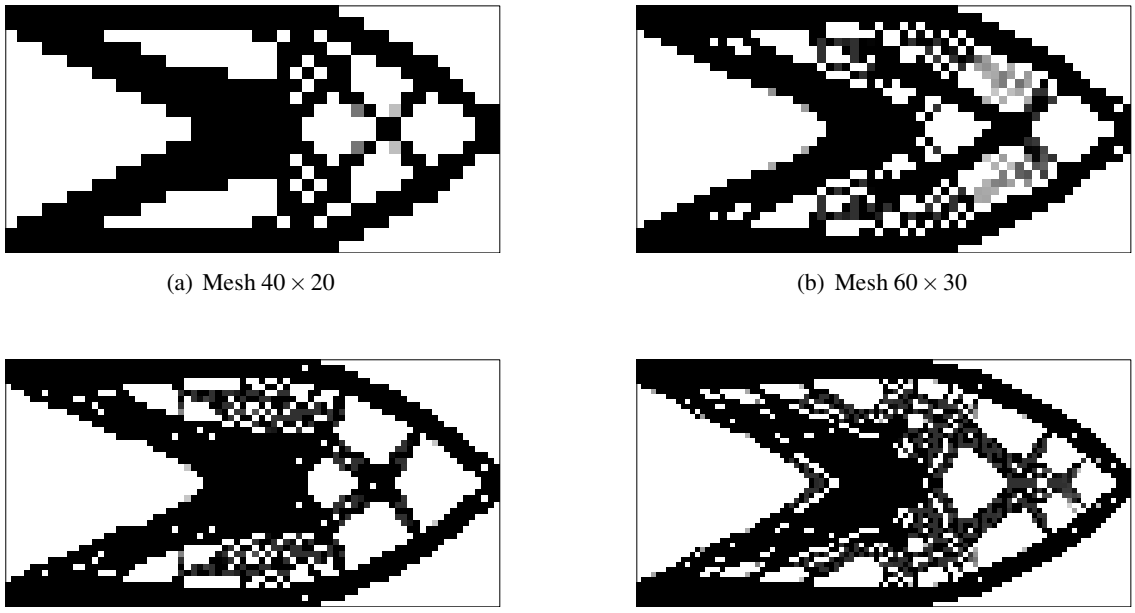

(a) Mesh 40×20 (b) Mesh 60×30

(c) Mesh 80×40 (d) Mesh 100×50

Figure 11: Optimal topologies for the short cantilever problem using the bilateral sensitivity filtering method.

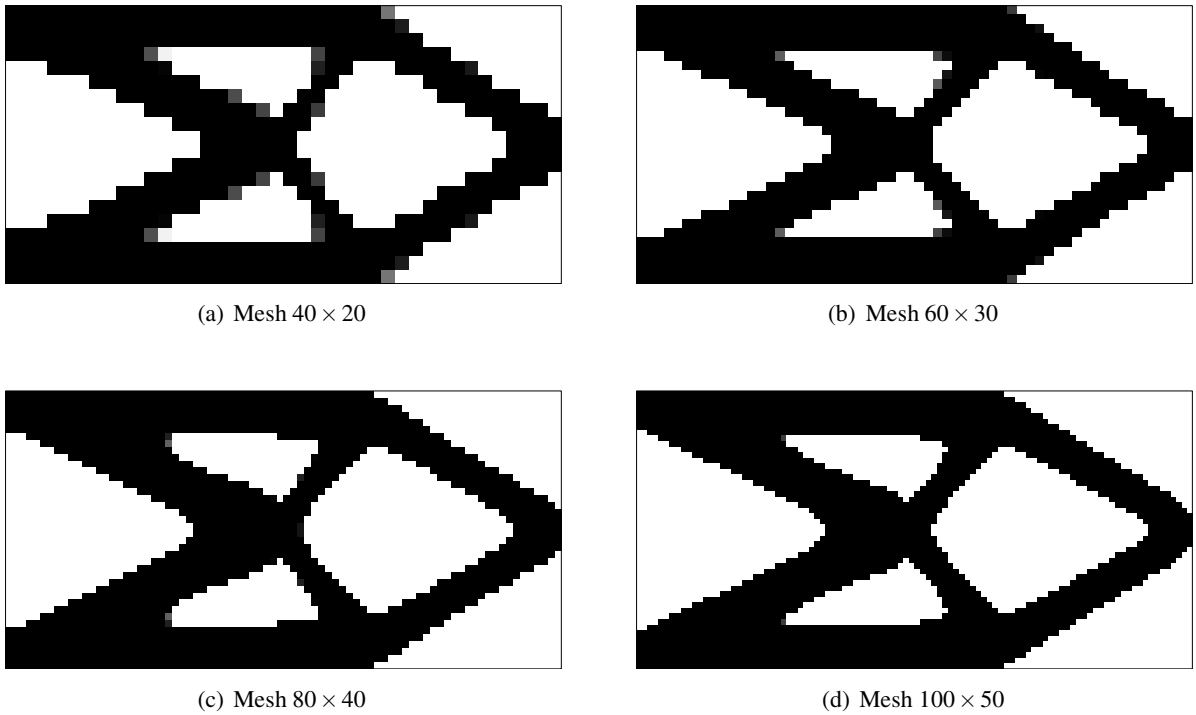

(a) Mesh 40×20 (b) Mesh 60×30

(c) Mesh 80×40 (d) Mesh 100×50

Figure 12: Optimal topologies for the short cantilever problem using the present hybrid sensitivity filtering method.

Table 2: Solutions to the short cantilever problem using different sensitivity filtering approaches.

Mesh	Approach	$J_{\min}$	ρ^*	Iterations	$\bar{t}_{\text{it}}$	$\bar{t}_{\text{fil}}$	$\bar{t}_{\text{frac}}$
40×20	Traditional	67.022	0.692	47	0.444	0.042	0.0952
	Bilateral	67.803	0.994	35	0.433	0.065	0.1496
	Hybrid	63.142	0.975	100	0.415	0.045	0.1086
60×30	Traditional	67.565	0.701	83	1.058	0.090	0.0848
	Bilateral	71.127	0.960	100	1.075	0.135	0.1260
	Hybrid	62.801	0.992	89	1.031	0.093	0.0906
80×40	Traditional	67.596	0.689	100	2.451	0.183	0.0748
	Bilateral	71.065	0.982	100	2.570	0.327	0.1271
	Hybrid	62.809	0.999	100	2.409	0.177	0.0733
100×50	Traditional	67.489	0.698	100	5.093	0.327	0.0642
	Bilateral	72.470	0.962	100	5.176	0.512	0.0989
	Hybrid	62.555	1.000	57	5.023	0.319	0.0634

$r_{\min} = 0.01$ and four different meshes. Again, it demonstrates that the traditional approach produces checkerboard-free and mesh-independent designs with poor 0-1 convergence at the shape boundaries. Figure 15 shows the optimal topologies generated by the present hybrid sensitivity filtering approach. The present approach can produce not only checkerboard-free and mesh-independent but also 0-1 convergent designs. The distinct ability of the present approach is again demonstrated. Table 3 displays the a comparison on the accuracy and efficiency between the traditional and the present hybrid sensitivity filtering approaches. Again, it shows that the present approach would be more accurate and efficient than the traditional approach and the sensitivity filtering is economical to overcome the numerical instabilities.

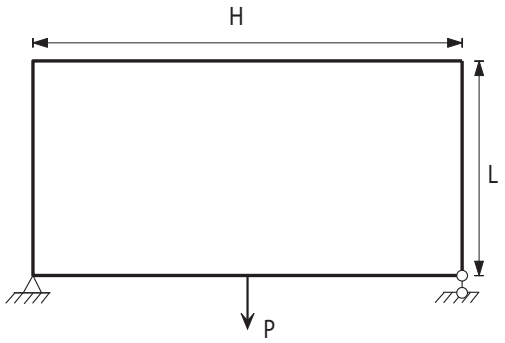

Figure 13: A 2D bridge topology optimization problem.

7.4 MBB Beam

The minimum compliance design problem of a MBB beam is used to further illustrate the accuracy and efficiency of the present hybrid sensitivity filtering approach. The MBB beam as shown in Fig. 16 is loaded with a concentrated vertical force of P at the centre of the top edge and is supported on rollers at the bottom-right corner and on fixed supports at the bottom-left corner. The basic parameters are assumed to be: $L = 3$, $H = 1$, thickness $t = 1.0$, load $P = 1$ and a volume fraction of 0.5.

Figure 17 shows the optimal designs for this problem produced by the traditional sensitivity filtering approach with a relatively large filter window size of $r_{\min} = 0.1$. It can be seen that checkerboard-free and mesh-independent designs are achieved, but the final designs can be quite blurry at the boundaries.Figure 18 shows the optimal designs generated by the present approach. The ability of the present approach in achieving checkerboard-free, mesh-independent and practical black-and-white designs is demonstrated again. The accuracy and efficiency of the present approach is further shown in Table 4. It can be seen that the present approach may be more accurate and efficient than the traditional approach. Evidently, the present approach for topology optimization can be highly competitive due to its high accuracy and efficiency.

Figure 19 shows the checkerboard-free and mesh-independent designs generated by the traditional sensitivity filtering approach with a smaller filter window size of $r_{\min} = 0.0533$. Due to the reduction in the filter radius as well as the smoothing effect, the optimal topologies become more complicated and the transition regions with intermediate densities occur inside the material domain in the final designs. The existence of these transition regions may hamper the identification of holes and cause difficulties in boundary identification and design realization in a post-processing step which is necessary for shape recovery from the optimization solution [Bendsøe and Sigmund (2003); Wang and Wang (2005); Sigmund (2007)]. In the SIMP method topology optimization using the traditional sensitivity filtering approach [Sigmund (2001a); Bendsøe and Sigmund (2003)], further hole identification was actually left to the users since there is no rigorous definition of a hole, one of the most important concepts in topology optimization. The present image-processing-based hole identification technique, as shown in Fig. 2, is thus applied to obtain the distinctly defined holes. Figure 20 shows the optimal topologies identified by the present hole identification technique, in which the identified holes are highlighted with black color. It can be seen the that the optimal topologies are also checkerboard-free

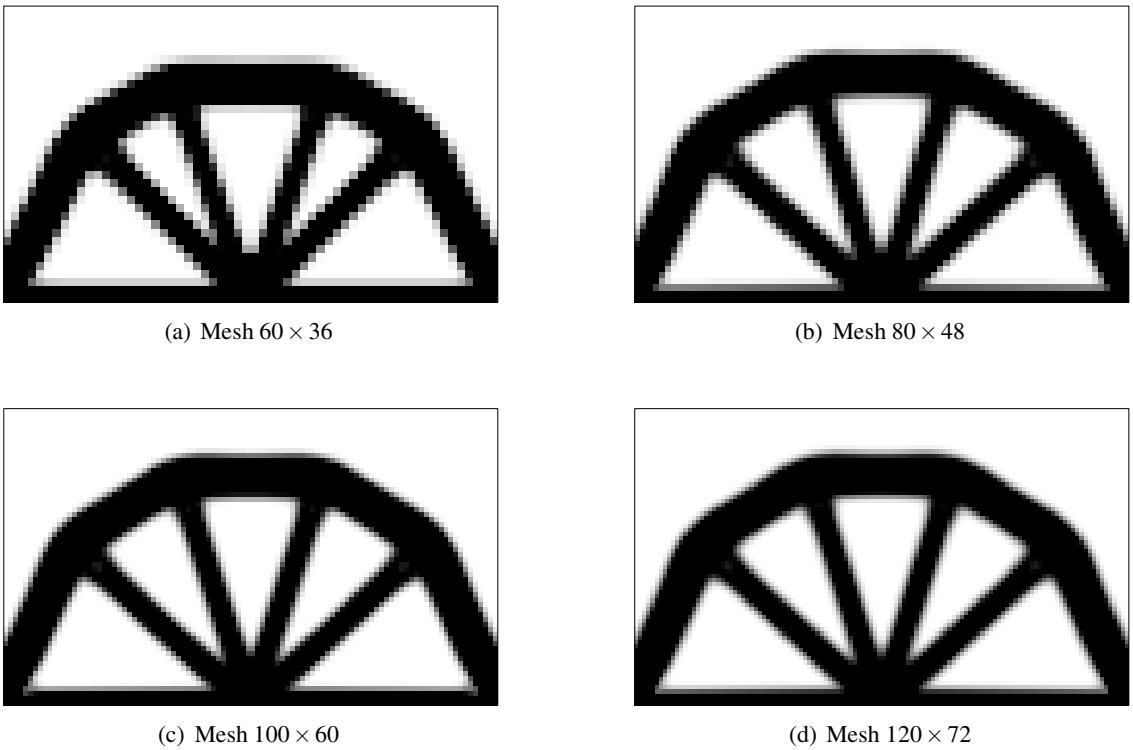

(a) Mesh 60×36 (b) Mesh 80×48

(c) Mesh 100×60 (d) Mesh 120×72

Figure 14: Optimal topologies for the 2D bridge problem using the traditional sensitivity filtering approach.

Table 3: Solutions to the 2D bridge problem using different sensitivity filtering approaches.

Mesh	Approach	$J_{\min}$	ρ^*	Iterations	$\bar{t}_{\text{it}}$	$\bar{t}_{\text{fil}}$	$\bar{t}_{\text{frac}}$
60×36	Traditional	14.603	0.702	58	1.346	0.111	0.0821
	Hybrid	13.921	0.967	100	1.371	0.113	0.0826
80×48	Traditional	15.178	0.685	100	3.206	0.193	0.0600
	Hybrid	14.339	0.990	100	3.210	0.193	0.0600
100×60	Traditional	15.354	0.717	100	6.809	0.347	0.0510
	Hybrid	14.782	0.993	66	6.700	0.331	0.0495
120×72	Traditional	15.756	0.685	100	12.774	0.491	0.0384
	Hybrid	15.001	0.999	66	12.970	0.470	0.0363

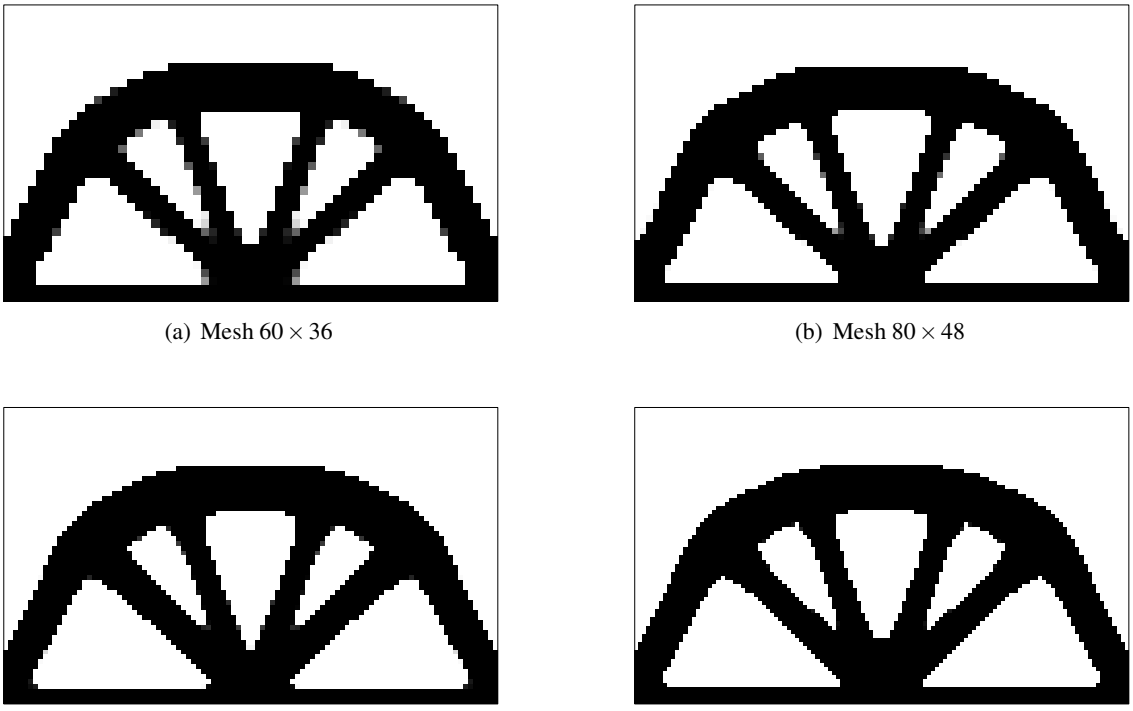

(a) Mesh 60×36 (b) Mesh 80×48

(c) Mesh 100×60 (d) Mesh 120×72

Figure 15: Optimal topologies for the 2D bridge problem using the present hybrid sensitivity filtering approach.

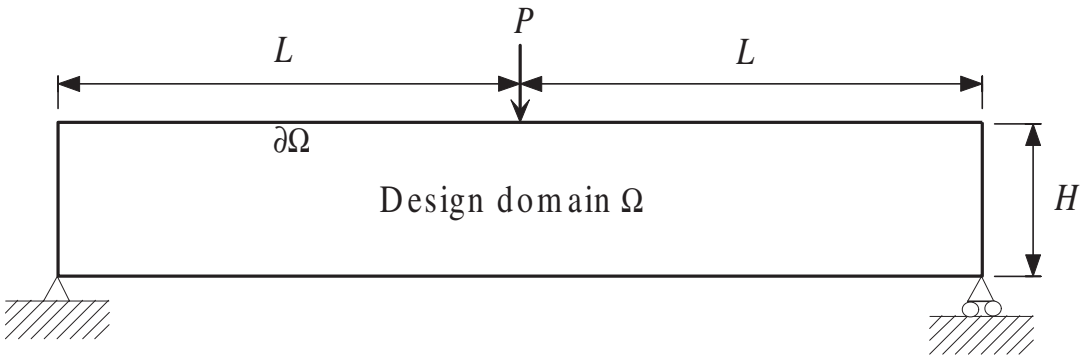

Figure 16: A MBB beam topology optimization problem.

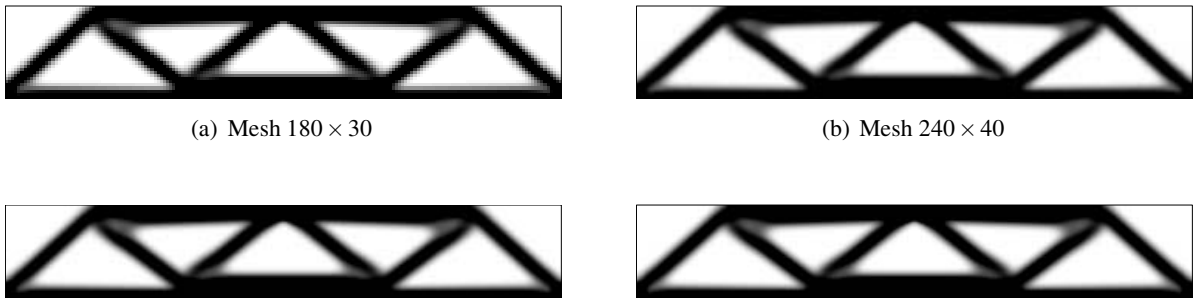

(a) Mesh 180×30 (b) Mesh 240×40

(c) Mesh 300×50 (d) Mesh 360×60

Figure 17: Optimal topologies for the MBB beam problem using the traditional sensitivity filtering approach ($r_{\min} = 0.1$).

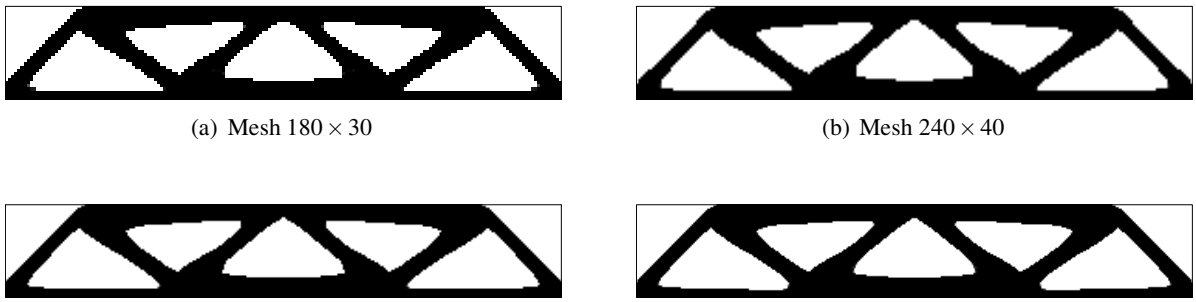

(a) Mesh 180×30 (b) Mesh 240×40

(c) Mesh 300×50 (d) Mesh 360×60

Figure 18: Optimal topologies for the MBB beam problem using the present hybrid sensitivity filtering approach ($r_{\min} = 0.1$).

Table 4: Solutions to the MBB beam problem using different sensitivity filtering approaches ($r_{\min} = 0.1$).

Mesh	Approach	$J_{\min}$	ρ^*	Iterations	$\overline{t}_{\text{it}}$	$\overline{t}_{\text{fil}}$	$\overline{t}_{\text{frac}}$
180×30	Traditional	105.687	0.662	100	4.974	0.345	0.0693
	Hybrid	96.362	0.999	100	5.430	0.357	0.0658
240×40	Traditional	106.399	0.650	100	13.170	0.709	0.0538
	Hybrid	96.605	1.000	73	14.627	0.702	0.0480
300×50	Traditional	106.837	0.648	90	30.071	1.352	0.0450
	Hybrid	96.433	1.000	74	32.779	1.246	0.0380
360×60	Traditional	107.051	0.649	100	58.722	2.355	0.0401
	Hybrid	96.657	1.000	89	64.637	2.079	0.0322

and mesh-independent (except the one in which the coarsest mesh 180×30 is used), however, existence of solutions may not be ensured rigorously since the minimum hole size is not exactly controlled by the minimum length-scale defined by the filter radius $r_{\min} = 0.0533$ due to the intermediate densities at the blurry boundaries.

Figure 21 shows the optimal designs produced by the present hybrid sensitivity filtering approach with the filter radius $r_{\min} = 0.0533$. The corresponding optimal topologies identified by the present hole identification technique are shown in Fig. 22. It can be seen that the final designs can be checkerboard-free, mesh-independent and mostly black-and-white, but transition regions with intermediate densities may exist and thus the present image-processing-based hole identification technique may be needed to obtain the mesh-independent holes, as shown in Fig. 22. Existence of solutions can be ensured more rigorously since the minimum hole size can be more accurately estimated due to the distinct boundaries of mesh-independent holes. Complete black-and-white designs cannot be achieved due to the use of the traditional sensitivity filter to smooth out the mesh-dependent holes. Figure 21 also shows the effect of mesh-refinement on the transition regions. It can be seen that finer meshes may lead to lower densities inside some transition regions. Since the distribution of element strain energy in a transition region controlled by the filter radius may become much smoother due to mesh-refinement, the filtered sensitivity of a low density element may be less amplified by the traditional sensitivity filter (13) and thus the tendency of 0-1 convergence will be less delayed. Nevertheless, it should be noted that creating new mesh-independent holes due to mesh-refinement cannot be guaranteed in general.

Comparing Fig. 21 with 19 as well as Fig. 22 with 20, it can be seen that the final topologies produced by the traditional approach may be quite different from those generated by the present approach. The minimum length-scale constraint on the structural member size may be strong enough to eliminate some small-size structural members to ruin the structural topology. Moreover, the unnecessary smoothing on mesh-independent holes may make the material distribution less effective and thus creation of new mesh-independent holes becomes easier. As a result, as shown in Figs. 19 and 20, the side effects of the traditional sensitivity filtering approach may lead to undesirable topological changes. Therefore, the present approach for topology optimization can be more accurate since the side effects can be well alleviated and the risk of converging to a sub-optimal solution can be avoided. Furthermore, a comparison on the accuracy and efficiency between these two approaches is listed in Table 5. It can be seen that the present approach may be more accurate and efficient in achieving black-and-white designs and both approaches may require relatively little CPU time in the SIMP method topology optimization.

Figure 23 shows the checkerboard-free and mesh-independent designs generated by the traditional sensitivity filtering approach with a smaller filter window size of $r_{\min} = 0.04$. Again, due to the further reduction in the filter radius, the optimal topologies become much more complicated. The blurry designs in Fig. 23 may cause difficulty in boundary identification and design realization in a post-processing step. Figure 24 shows the optimal topologies identified by the present hole identification technique. The identified optimal topologies can also be mesh-independent, but the minimum hole size constraint may be inaccurately satisfied. Figure 25 displays the checkerboard-free and mostly black-and-white designs produced by the present constrained sensitivity filtering approach. It can be seen that mesh-independent designs can be obtained provided the finite element meshes are fine enough. The corresponding optimal topologies identified by the present hole identification technique are shown in Fig. 26. The minimum hole size constraint can be more accurately satisfied and existence of solutions can be more rigorously ensured. Again, it shows that mesh-independent topologies can be achieved only if the finite element meshes are fine enough. In this sense, the computational cost may become higher, but the minimum hole size constraint controlled by the filter radius can be more accurately satisfied and thus existence of solu-

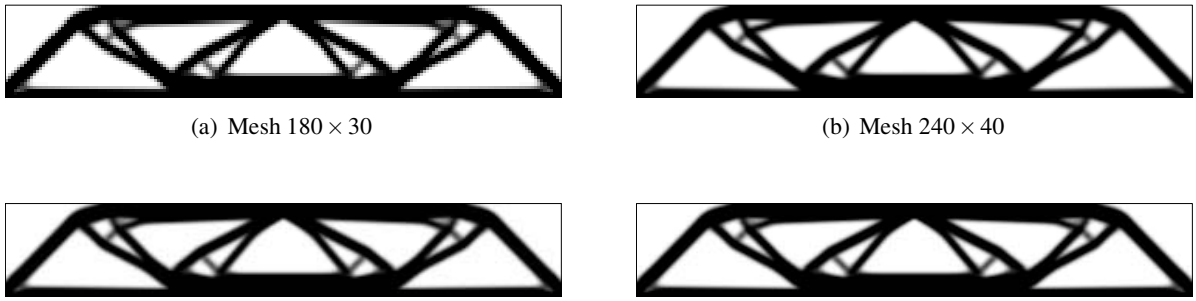

(a) Mesh 180×30 (b) Mesh 240×40

(c) Mesh 300×50 (d) Mesh 360×60

Figure 19: Optimal designs for the MBB beam problem using the traditional sensitivity filtering approach ($r_{\min} = 0.0533$).

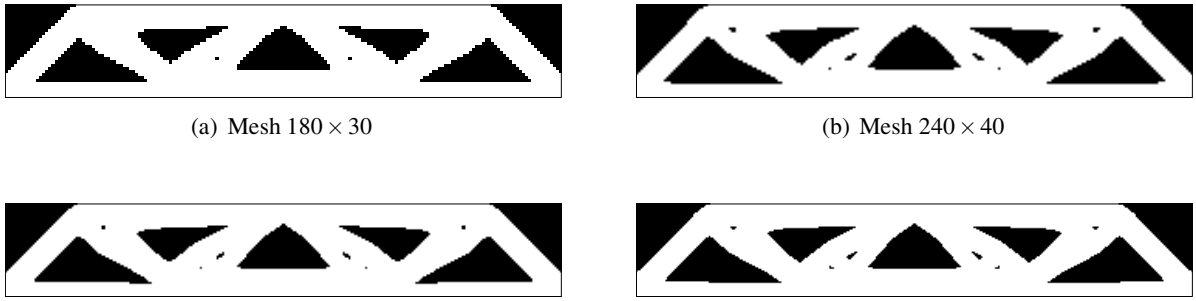

(a) Mesh 180×30 (b) Mesh 240×40

(c) Mesh 300×50 (d) Mesh 360×60

Figure 20: Optimal topologies using the traditional sensitivity filtering approach ($r_{\min} = 0.0533$) identified by the present hole identification technique.

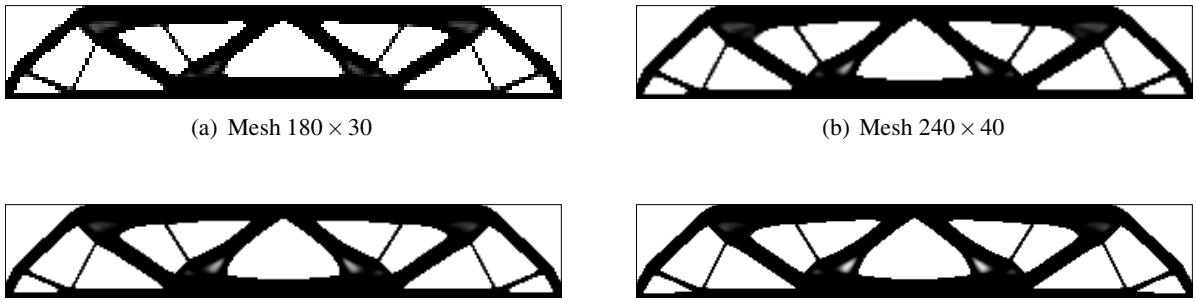

(a) Mesh 180×30 (b) Mesh 240×40

(c) Mesh 300×50 (d) Mesh 360×60

Figure 21: Optimal designs for the MBB beam problem using the present hybrid sensitivity filtering approach ($r_{\min} = 0.0533$).

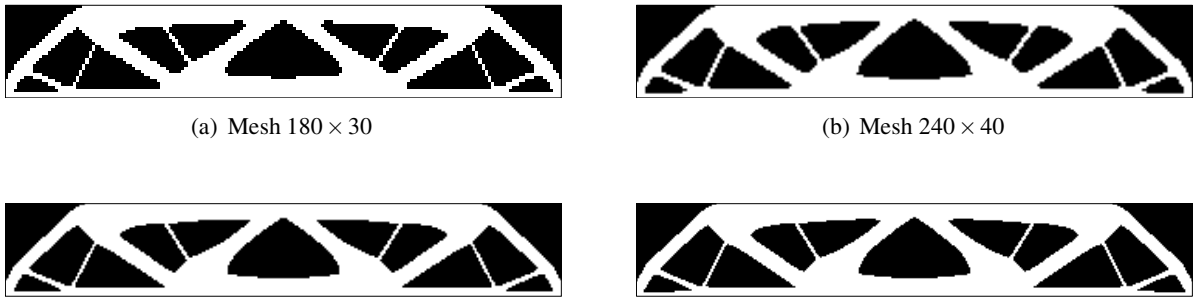

(a) Mesh 180×30 (b) Mesh 240×40

(c) Mesh 300×50 (d) Mesh 360×60

Figure 22: Optimal topologies using the present hybrid sensitivity filtering approach ($r_{\min} = 0.0533$) identified by the present hole identification technique.

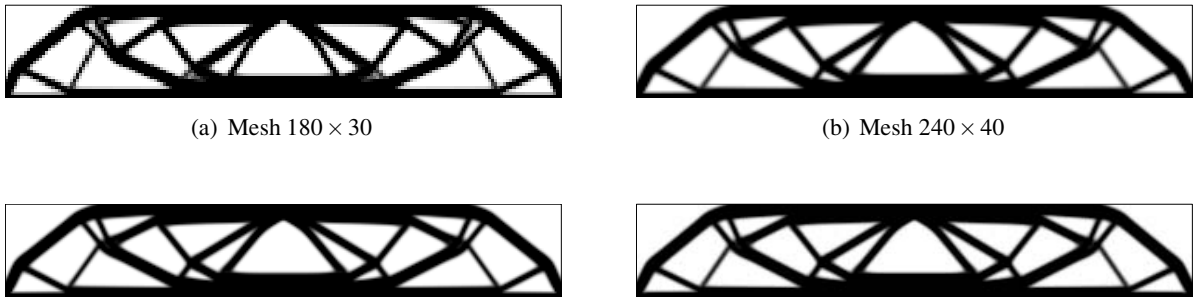

(a) Mesh 180×30 (b) Mesh 240×40

(c) Mesh 300×50 (d) Mesh 360×60

Figure 23: Optimal designs for the MBB beam problem using the traditional sensitivity filtering approach ($r_{\min} = 0.04$).

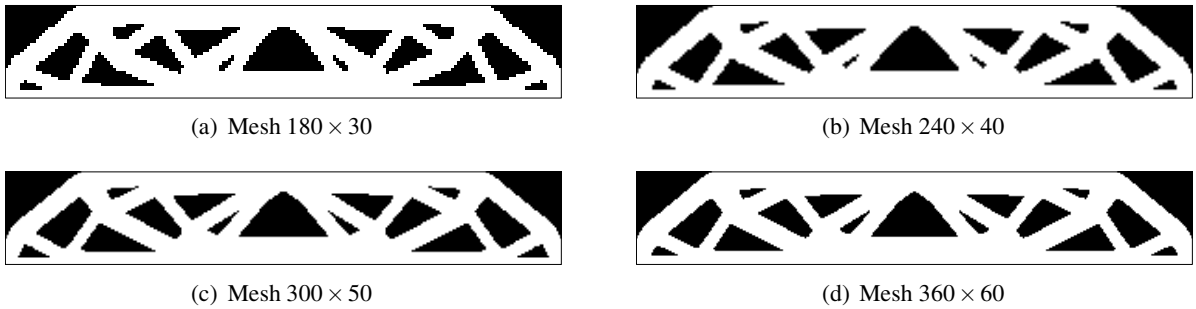

(a) Mesh 180×30 (b) Mesh 240×40

(c) Mesh 300×50 (d) Mesh 360×60

Figure 24: Optimal topologies for the MBB beam problem using the traditional sensitivity filtering approach ($r_{\min} = 0.04$) identified by the present hole identification technique.

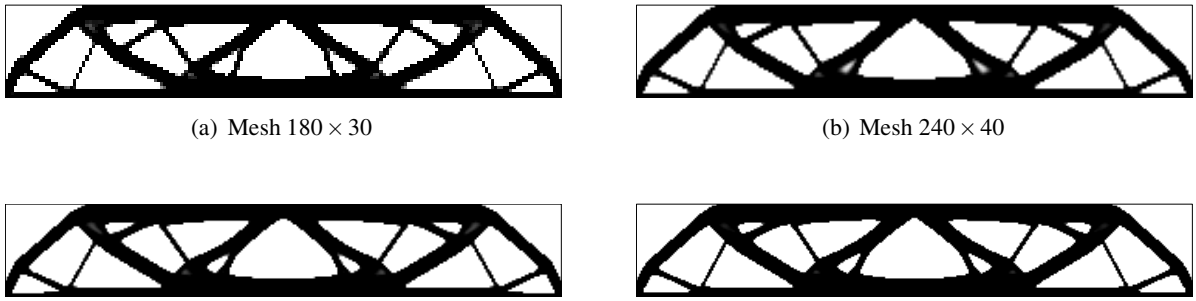

(a) Mesh 180×30 (b) Mesh 240×40

(c) Mesh 300×50 (d) Mesh 360×60

Figure 25: Optimal topologies for the MBB beam problem using the present hybrid sensitivity filtering approach ($r_{\min} = 0.04$).

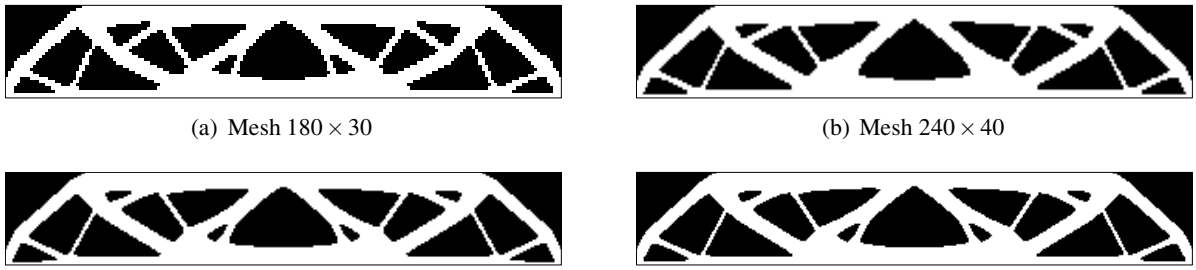

(a) Mesh 180×30 (b) Mesh 240×40

(c) Mesh 300×50 (d) Mesh 360×60

Figure 26: Optimal topologies for the MBB beam problem using the present hybrid sensitivity filtering approach ($r_{\min} = 0.04$) identified by the present hole identification technique.

Table 5: Solutions to the MBB beam problem using different sensitivity filtering approaches ($r_{\min} = 0.0533$).

Mesh	Approach	$J_{\min}$	ρ^*	Iterations	$\overline{t}_{\text{it}}$	$\overline{t}_{\text{fil}}$	$\overline{t}_{\text{frac}}$
180×30	Traditional	100.244	0.717	100	4.973	0.269	0.0540
	Hybrid	95.174	0.973	100	5.336	0.289	0.0541
240×40	Traditional	100.207	0.730	100	13.846	0.536	0.0387
	Hybrid	95.613	0.969	50	14.563	0.562	0.0386
300×50	Traditional	101.048	0.720	100	30.652	0.845	0.0276
	Hybrid	95.532	0.990	94	32.488	0.841	0.0259
360×60	Traditional	101.145	0.721	100	61.203	1.431	0.0234
	Hybrid	95.824	0.988	95	64.483	1.366	0.0212

Table 6: Solutions to the MBB beam problem using different sensitivity filtering approaches ($r_{\min} = 0.04$).

Mesh	Approach	$J_{\min}$	ρ^*	Iterations	$\bar{t}_{\text{it}}$	$\bar{t}_{\text{fil}}$	$\bar{t}_{\text{frac}}$
180×30	Traditional	97.304	0.725	54	5.554	0.272	0.0490
	Hybrid	94.061	0.949	62	5.228	0.295	0.0564
240×40	Traditional	97.847	0.718	100	13.911	0.460	0.0331
	Hybrid	94.701	0.985	100	14.408	0.497	0.0345
300×50	Traditional	97.414	0.743	100	30.568	0.828	0.0271
	Hybrid	94.965	0.989	60	32.020	0.858	0.0268
360×60	Traditional	98.117	0.719	100	60.989	1.203	0.0197
	Hybrid	95.152	0.997	66	64.049	1.236	0.0193

tions may be more rigorously ensured. Comparing Fig. 26 with Fig. 24, it can be seen that the optimal topologies generated by the present and traditional approaches can be nearly identical. A further comparison on the accuracy and efficiency between these two approaches is listed in Table 6. It can be seen that the present approach may be more accurate than the traditional approach with similar or far less total CPU time to reach the convergence. Again, the high accuracy and efficiency of the present approach are demonstrated.

8 Conclusions

In this study, an accurate and efficient hybrid sensitivity filtering approach based on the traditional and the bilateral sensitivity filtering approaches is proposed for topology optimization. In producing checkerboard-free, mesh-independent and black-and-white designs, the traditional and the bilateral sensitivity filtering approaches have their respective advantages and drawbacks. The traditional approach can overcome the numerical instabilities robustly, but the structural boundary may be permanently blurred. The bilateral approach can drive the 0-1 convergence globally, but the numerical instabilities may be not fully eliminated. The present hybrid approach combines the traditional approach to overcome the numerical instabilities with the bilateral approach to favor the occurrence of distinct boundaries of mesh-independent holes. The traditional sensitivity filter is only applied to a sub-domain where the numerical instabilities are likely to occur, the bilateral sensitivity filter is employed for the corresponding nearest neighboring elements of mesh-independent holes and no filtering is introduced for mesh-independent holes. As a result, the numerical instabilities can be robustly suppressed and distinct boundaries of mesh-independent holes can be achieved. Existence of solutions can be ensured more accurately and the side effects of both the traditional and the bilateral sensitivity filters can be avoided or alleviated. The present approach can achieve not only checkerboard-free and mesh-independent but also mostly black-and-white designs. Furthermore, the present approach is computationally efficient because filtering is prohibited in the usually large non-filtering sub-domain. Therefore, the present approach can be both accurate and efficient for the SIMP method topology optimization. The high accuracy and efficiency of the present approach are illustrated with classical examples in minimum compliance design. It is suggested that the present approach for topology optimization be highly appealing.

References

Bendsøe, M. P. (1989): Optimal shape design as a material distribution problem. *Structural Optimization*, vol. 1, pp. 193–202.

Bendsøe, M. P. (1995): *Optimization of structural topology, shape and material*. Springer, Berlin, Heidelberg, New York.

Bendsøe, M. P.; Kikuchi, N. (1988): Generating optimal topologies in structural design using

a homogenization method. *Computer Methods in Applied Mechanics and Engineering*, vol. 71, pp. 197–224.

Bendsøe, M. P.; Sigmund, O. (1999): Material interpolations in topology optimization. *Archive of Applied Mechanics*, vol. 69, pp. 635–654.

Bendsøe, M. P.; Sigmund, O. (2003): *Topology Optimization: Theory, Methods and Applications*. Springer-Verlag, Berlin.

Borrval, T. (2001): Topology optimization of elastic continua using restriction. *Archives of Computational Methods in Engineering*, vol. 8, no. 4, pp. 351–385.

Bourdin, B. (2001): Filters in topology optimization. *International Journal for Numerical Methods in Engineering*, vol. 50, pp. 2143–2158.

Bruns, T. E.; Tortorelli, D. A. (2001): Topology optimization of non-linear elastic structures and compliant mechanisms. *Computer methods in Applied Mechanics and Engineering*, vol. 190, no. 26–27, pp. 3443–3459.

Bulman, S.; Sienz, J.; Hinton, E. (2001): Comparisons between algorithms for structural topology optimization using a series of benchmark studies. *Computers & Structures*, vol. 79, no. 12, pp. 1203–1218.

Cardoso, E. L.; Fonseca, J. S. O. (2003): Complexity control in the topology optimization of continuum structures. *Journal of the Brazilian Society of Mechanical Sciences and Engineering*, vol. 25, no. 3, pp. 293–301.

Chang, F.; Chen, C.-J.; Lu, C.-J. (2004): A linear-time component-labeling algorithm using contour tracing technique. *Computer Vision and Image Understanding*, vol. 93, no. 2, pp. 206–220.

Cisilino, A. P. (2007): Topology optimization of 2D potential problems using boundary elements. *CMES: Computer Modeling in Engineering & Sciences*, vol. 15, no. 2, pp. 99–106.

Durand, F.; Dorsey, J. (2002): Fast bilateral filtering for the display of high-dynamic-range images. In *Proc. ACM Conference on Computer Graphics (SIGGRAPH)*, pp. 257–266, San Antonio, USA.

Elad, M. (2002): On the origin of the bilateral filter and ways to improve it. *IEEE Transactions on Image Processing*, vol. 11, no. 10, pp. 1141–1151.

Eschenauer, H. A.; Olhoff, N. (2001): Topology optimization of continuum structures: A review. *Applied Mechanics Review*, vol. 54, no. 4, pp. 331–390.

Fleishman, S.; Drori, I.; Cohen, D. (2003): Bilateral mesh denoising. In *Proc. SIGGRAPH*, pp. 950–953.

Jahne, B. (1997): *Digital Image Processing - Concepts, Algorithms, and Scientific Applications*. Springer-Verlag, Berlin, 4th edition.

Jang, G.-W.; Jeong, J. H.; Kim, Y. Y.; Sheen, D.; Park, C.; Kim, M.-N. (2003): Checkerboard-free topology optimization using non-conforming finite elements. *International Journal for Numerical Methods in Engineering*, vol. 57, pp. 1717–1735.

Jiang, W.; Baker, M. L.; Wu, Q.; Bajaj, C.; Chiua, W. (2003): Applications of a bilateral denoising filter in biological electron microscopy. *Journal of Structural Biology*, vol. 144, pp. 114–122.

Michell, A. G. M. (1904): The limits of economy of material in frame-structures. *Philosophical Magazine*, vol. 8, no. 6, pp. 589–597.

Petersson, J. (1999): Some convergence results in perimeter-controlled topology optimization. *Computer Methods in Applied Mechanics and Engineering*, vol. 171, pp. 123–140.

Petersson, J.; Sigmund, O. (1998): Slope constrained topology optimization. *International Journal for Numerical Methods in Engineering*, vol. 41, pp. 1417–1434.

Rozvany, G.; Zhou, M. (1991): Applications of COC method in layout optimization. In Eschenauer, H.; Mattheck, C.; Olhoff, N.(Eds): *Proc. Conf. "Eng. Opt. in Design Processes"*, pp. 59–70, Berlin, Heidelberg, New York. Springer-Verlag.

Rozvany, G. I. N. (2001): Aims, scope, methods, history and unified terminology of computer-aided topology optimization in structural mechanics. *Structural and Multidisciplinary Optimization*, vol. 21, no. 2, pp. 90–108.

Rozvany, G. I. N.; Zhou, M.; Birker, T. (1992): Generalized shape optimization without homogenization. *Strutural Optimization*, vol. 4, pp. 250–254.

Sigmund, O. (1994): *Design of material structures using topology optimization*. PhD thesis, Technical University of Denmark, 1994.

Sigmund, O. (1997): On the design of compliant mechanisms using topology optimization. *Mechanics of Structures and Machines*, vol. 25, no. 4, pp. 495–526.

Sigmund, O. (2001): A 99 line topology optimization code written in MATLAB. *Structural and Multidisciplinary Optimization*, vol. 21, no. 2, pp. 120–127.

Sigmund, O. (2001): Design of multiphysics actuators using topology optimization - Part II: two-material structures. *Computer Methods in Applied Mechanics and Engineering*, vol. 49–50, no. 190, pp. 6605–6627.

Sigmund, O. (2007): Morphology-based black and white filters for topology optimization. *Structural and Multidisciplinary Optimization*, vol. 33, pp. 401–424.

Sigmund, O.; Petersson, J. (1998): Numerical instabilities in topology optimization: A survey on procedures dealing with checkerboards, mesh-independencies and local minima. *Structural Optimization*, vol. 16, pp. 68–75.

Stolpe, M.; Svanberg, K. (2003): Modelling topology optimization problems as linear mixed 0–1 programs. *International Journal for Numerical Methods in Engineering*, vol. 57, no. 5, pp. 723–739.

Tapp, C.; Hansel, W.; Mittelstedt, C.; Becker, W. (2004): Weight-minimization of sandwich structures by a heuristic topology optimization algorithm. *CMES: Computer Modeling in Engineering & Sciences*, vol. 5, no. 6, pp. 563–574.

Tomasi, C.; Manduchi, R. (1998): Bilateral filtering for gray and color images. In *Proceedings of the 1998 IEEE International Conference on Computer Vision*, pp. 839–846, Bombay, India.

Wang, M. Y.; Wang, S. Y. (2005): Bilateral filtering for structural topology optimization. *International Journal for Numerical Methods in Engineering*, vol. 63, no. 13, pp. 1911–1938.

Wang, M. Y.; Wang, X. (2004): PDE-driven level sets, shape sensitivity and curvature flow for structural topology optimization. *CMES: Computer Modeling in Engineering & Sciences*, vol. 6, no. 4, pp. 373–396.

Wang, M. Y.; Zhou, S. (2004): Phase field: A variational method for structural topology optimization. *CMES: Computer Modeling in Engineering & Sciences*, vol. 6, no. 6, pp. 547–566.

Wang, S. Y.; Lim, K. M.; Khoo, B. C.; Wang, M. Y. (2007): An extended level set method for shape and topology optimization. *Journal of Computational Physics*, vol. 221, no. 1, pp. 395–421.

Wang, S. Y.; Lim, K. M.; Khoo, B. C.; Wang, M. Y. (2007): A geometric deformation constrained level set method for structural shape and topology optimization. *CMES: Computer Modeling in Engineering & Sciences*, vol. 18, no. 3, pp. 155–182.

Wang, S. Y.; Lim, K. M.; Khoo, B. C.; Wang, M. Y. (2007): On hole nucleation in topology optimization using the level set methods. *CMES: Computer Modeling in Engineering & Sciences*, vol. 21, no. 3, pp. 219–238.

Wang, S. Y.; Lim, K. M.; Khoo, B. C.; Wang, M. Y. (2007): An unconditionally time-stable level set method and its application to shape and topology optimization. *CMES: Computer Modeling in Engineering & Sciences*, vol. 21, no. 1, pp. 1–40.

Wang, S. Y.; Tai, K. (2004): Graph representation for evolutionary structural topology optimization. *Computers & Structures*, vol. 82, no. 20–21, pp. 1609–1622.

Wang, S. Y.; Tai, K. (2005): Bar-system representation method for structural topology optimization using the genetic algorithms. *Engineering Computations*, vol. 22, no. 2, pp. 206–231.

Wang, S. Y.; Tai, K. (2005): Structural topology design optimization using genetic algorithms with a bit-array representation. *Computer Methods in Applied Mechanics and Engineering*, vol. 194, no. 36–38, pp. 3749–3770.

Wang, S. Y.; Tai, K.; Quek, S. T. (2006): Topology optimization of piezoelectric sensors/actuators for torsional vibration control of composite plates. *Smart Materials and Structures*, vol. 15, pp. 253–269.

Wang, S. Y.; Tai, K.; Wang, M. Y. (2006): An enhanced genetic algorithm for structural topology optimization. *International Journal for Numerical Methods in Engineering*, vol. 65, no. 1, pp. 18–44.

Wang, S. Y.; Wang, M. Y. (2006): Structural shape and topology optimization using an implicit free boundary parametrization method. *CMES: Computer Modeling in Engineering & Sciences*, vol. 13, no. 2, pp. 119–147.

Xie, Y. M.; Steven, G. P. (1993): A simple evolutionary procedure for structural optimization. *Computers & Structures*, vol. 49, no. 5, pp. 885–896.

Zhou, J.; Hu, Q. M.; He, X. J. (2004): Edge detection with bilateral filtering in spiral space. In *Proceedings of the 2nd International Conference on Information Technology for Application (ICITA 2004)*, pp. 222–225.

Zhou, M.; Shyy, Y.; Thomas, H. (2001): Checkerboard and minimum member size control in topology optimization. *Structural and Multidisciplinary Optimization*, vol. 21, pp. 152–158.

Zhou, S.; Wang, M. Y. (2006): 3D multimaterial structural topology optimization with the generalized Cahn-Hilliard equations. *CMES: Computer Modeling in Engineering & Sciences*, vol. 16, no. 2, pp. 83–102.